Measurements and Modelling of Low-Frequency Disturbances in Induction Machines

Torbjörn Thiringer

Technical Report No. 151 L

1993

SCHOOL OF ELECTRICAL AND COMPUTER ENGINEERING

CHALMERS UNIVERSITY OF TECHNOLOGY

GÖTEBORG, SWEDEN

Measurements and Modelling of Low-Frequency Disturbances in Induction Machines

by

Torbjörn Thiringer

Technical Report No. 151 L

Submitted to the School of Electrical and Computer Engineering
Chalmers University of Technology
in partial fulfilment of the requirements
for the degree of
Licentiate of Engineering

Department of Electrical Machines and Power Electronics
Chalmers University of Technology
Göteborg, Sweden
June 1993

ISBN 91-7032-822-6
Vasastadens Bokbinderi AB
Göteborg 1993

ABSTRACT

In this thesis the low-frequency dynamic behaviour of the induction machine is analysed. Disturbances in the shaft torque and supply voltage are investigated theoretically. The calculated response to shaft torque disturbances is verified with measurements on a 15 kW machine. Furthermore, the influence of the machine parameters, skin effect and operating-point is studied. The results predicted using some models of lower order are compared with measurements and results obtained by using a two-axis model. The results indicate that a first-order model can be used to determine the dynamic response to shaft torque and voltage disturbances up to one or a few hertz. By using a second-order model also higher disturbance frequencies can be treated with a rather small loss of accuracy. The temperature significantly effects the low-frequency dynamics of the induction machine while the influence of the skin effect and static shaft torque is of less importance to an ordinary industrial machine.

ACKNOWLEDGEMENT

I would like to express my gratitude to my supervisor Dr Jonny Hylander for all the encouragement and support given throughout the work on this thesis. Further, I would like to thank Professor Jorma Luomi, my examinator Dr Karl-Erik Hallenius and Dr Tore Svensson for many valuable suggestions and comments. I would also like to thank Margot Bolinder for linguistic help. The financial support given by the Swedish National Board for Industrial and Technical Development (NUTEK) is gratefully acknowledged.

CONTENTS

page

LIST OF SYMBOLS

Symbol	Meaning	Unit
A	numerical constant	
$a(s)$	transfer function denominator	
B	equivalent damper coefficient	Nms/rad
$b(s)$	transfer function numerator	
C	equivalent capacitance	F
c_i	numerical constant	
$G_{ij}(s)$	transfer function matrix element	
F	force	Nm
f	frequency	Hz
f_l	limit frequency for the damper model	Hz
f_s	supply frequency	Hz
f_0	undamped eigenfrequency	Hz
$h(t)$	impulse response, natural response	
$\underline{I}_r$	rotor current phasor referred to the stator side	A
$\underline{I}_s$	stator current phasor	A
i_a, i_a, i_c	phase currents	A
i_{ds}	stator current in d-axis	A
i_{dr}	rotor current in d-axis referred to the stator side	A
i_{qr}	rotor current in q-axis referred to the stator side	A
i_{qs}	stator current in q-axis	A
$\underline{i}_r$	rotor current vector referred to the stator side	A
$\underline{i}_s$	stator current vector	A
$H(s)$	transfer function	
J_m	machine inertia	kgm^2
J_t	wind turbine rotor inertia	kgm^2
j	imaginary unit	
K	numerical constant	
K	equivalent spring constant	Nm/rad
k	constant for simplification of the steady-state equivalent circuit	
L	equivalent inductance	H
L_m	magnetizing inductance	H
L_r	rotor inductance referred to the stator side	H
L'_r	rotor transient inductance referred to the stator side	H

$L_{r\lambda}$	rotor leakage inductance referred to the stator side	H
L_s	stator inductance	H
L'_s	stator transient inductance	H
$L_{s\lambda}$	stator leakage inductance	H
n	rotor speed	rpm
n	system order	
P_{Cus}	stator resistance losses	W
P_e	electrical power	W
P_{Fes}	core losses in the stator	W
P_i	pole	
P_n	rated power	W
P_δ	air gap power	W
p	pole pair number	
R	equivalent resistance	Ω
R_{cl}	equivalent resistance to represent core losses	Ω
R_k	locked-rotor resistance	Ω
R_r	rotor resistance referred to the stator side	Ω
R_s	stator resistance	Ω
R_0	equivalent resistance	Ω
S	slip	
s	Laplace operator	
T_e	electrodynamical torque	Nm
T_n	rated torque	Nm
T_{ref}	reference torque signal	Nm
T_s	shaft torque	Nm
T_{wind}	wind torque	Nm
U	voltage	V
U_{ph}	phase voltage	V
U_n	rated voltage	V
U_q	voltage in the q-direction	V
U_0	equivalent voltage	V
u_a, u_b, u_c	phase voltages	V
$\underline{u}_s$	stator voltage vector	V
X_m	magnetizing reactance	Ω
$X_{r\lambda}$	rotor leakage reactance	Ω
$X_{s\lambda}$	stator leakage reactance	Ω
X_0	equivalent reactance	Ω
Z_i	zero	

$\mathbf{A}$	system matrix	
$\mathbf{B}$	input matrix	
$\mathbf{C}$	output matrix	
$\mathbf{D}$	direct matrix	
$\mathbf{G}$	transfer function matrix	
$\mathbf{I}$	identity matrix	
$\mathbf{I}$	current vector	A
$\mathbf{L}$	inductance matrix	H
$\mathbf{R}$	resistance matrix	Ω
$\mathbf{U}$	voltage vector	V
$\mathbf{U}$	Laplacetransformed input vector	
$\mathbf{u}$	input vector	
$\mathbf{Y}$	Laplacetransformed output vector	
$\mathbf{y}$	output vector	
$\mathbf{x}$	state vector	
α	torsional stiffness	Nm/rad
ε	relative disturbance amplitude	
λ_i	eigenvalue	
ξ	damping ratio	
σ	real constant	
$\underline{\Psi}_r$	rotor flux vector	Vs
$\underline{\Psi}_s$	stator flux vector	Vs
Ω_m	mechanical rotor speed	rad/s
ω	constant	
ω_k	angular velocity of coordinate system	rad/s
ω_s	supply angular frequency	rad/s
ω_{s0}	steady-state supply angular frequency	rad/s
ω_0	undamped natural angular frequency	rad/s

1 INTRODUCTION

Electric power pulsations from two-bladed wind turbines have been observed with a frequency twice the rotational frequency of the wind turbine. One reported example is the 2.4 MW wind turbine situated at Näsudden on the Island of Gotland in the Baltic Sea [1]. This wind turbine is equipped with an induction machine which in certain frequency regions can amplify shaft torque disturbances. It has been suggested by Hinrichsen et al. [2] and Chan et al. [3] that these shaft torque pulsations could be caused by the wind shear (different wind speeds at different heights) or by aerodynamical effects when the blades pass the tower. Other examples, where shaft torque pulsations have been reported, are compressor drives. Since the commonly used dynamic representation of the induction machine is a fifth-order non-linear system, numerical simulations must often be performed to analyse these situations. If the phase currents are of interest, such a detailed model will be needed. However, it is possible to use a simpler model, if the rotor speed and electrodynamical torque perturbations due to low-frequency pulsations in the shaft torque and supply voltage are to be calculated. The need of simple but still reliable models increases when a larger system consisting of several machines is to be investigated. An example of such a multi-machine system is a wind farm.

Several papers have been presented on simplified induction machine models and on the low-frequency dynamic behaviour of the induction machine. Nacke [4] suggested that the induction machine could be represented by a spring, a mass and a damper. With this second-order model it is possible to determine the induction machine response to disturbances in the shaft torque. The induction machine is usually subcritically damped and the eigenfrequency is located in the region of 5-30 Hz. There is also another eigenfrequency, just below the supply frequency according to Lorenzen [5], but only the lower, often referred to as the dominating one, influences the response to shaft torque disturbances. The damping at the dominating eigenfrequency can be very poor, especially for large and low-slip induction machines according to Novotny et al. [6], or even non-existing. The possibility of self-excited oscillations for certain combinations of machine parameters, above all for high stator resistance, was investigated by Lorenzen [5, 7, 8] and Nelson et al. [9]. Palit [10] and Kron et al. [11] presented experiments in which the stator resistance was increased until the investigated induction machine started to self-oscillate.

Nacke [12] and Peterson [13] performed experiments in order to determine the damping ratio and eigenfrequency of the induction machine by supplying the stator with dc-current and in this way transforming the synchronous speed to zero. Peterson also found an additional lower resonance possibility at which increased stator resistance lead to reduced damping. At the dominating eigen-frequency, however, he found the opposite. Also Späth [14] suggested that the stator resistance improved the damping at the dominating eigenfrequency. However, the measurements presented were not compared with calculations. Leonhard [15] measured the electrodynamical torque response to shaft torque disturbances and obtained a good agreement between measured and calculated values. To determine the electrodynamical torque, the electrical power was measured with an instantaneous power meter consisting of Hall-elements. Späth as well as Leonhard performed the experiments on an induction machine connected to a 50 Hz grid.

The low-frequency dynamics of the machine is influenced by the skin effect, Lorenzen [16] and Langheim [17], and also by a varying static load, Nacke [12] and Kovacs [18]. Several authors have derived and investigated third-order numerical models based on the negligence of the fast stator transients. These models are not only capable of calculating disturbances in the shaft torque. Wasynczuk et al. [19] claimed that the response to perturbations in the amplitude of the supply voltage with a frequency up to the dominating eigenfrequency can be calculated.

The purpose of this thesis is to investigate the validity of some low-order induction machine models. The models are: a first-order model based on the equivalent circuit and a second-order model based on the negligence of the stator resistance. In order to do this, it is also important to have a good knowledge of the low-frequency behaviour of the induction machine. Thus, the influence of the stator resistance, operating-point, temperature and skin effect must be studied. To verify the calculations with measurements is also an objective. The ambition has been to give valuable information for the selection of an induction machine model to be used when analysing a larger system, for instance a wind turbine.

In **Chapter 2** the induction machine is analysed using linear theory, and the different models are derived. After presenting the measurement equipment and methods in **Chapter 3**, the models are compared with measurements in **Chapter 4**. In **Chapter 5** the dynamic influence of different factors such as varying machine parameters, different operating-points, skin effect in the rotor conductors and machine temperature is investigated. Finally, In **Chapter 6** an example of how the analysis of the drive train of a wind turbine can be simplified is presented.

2 THEORY

In this chapter, a short summary of the linear analysis necessary for the investigation is given selected from [20, 21]. The models to be used are also derived in this section as the theoretical background for each model has been presented.

2.1 Linear systems analysis

Many systems are non-linear and a non-linear numerical simulation must be performed in order to analyse these thoroughly, since the dynamics of the system may depend on the operating-point or the magnitude of the disturbance. Some non-linear systems of low order can be analysed analytically, but this is not the case with the induction machine. A generally used method to analyse a non-linear system is to linearize it around a certain operating-point and derive a linear small-perturbation model. The system can now be analysed using linear methods. However, caution must be taken in order to avoid extrapolation.

A linear system on state-space representation is usually described by

$$\frac{d}{dt}\mathbf{x} = \mathbf{A}\mathbf{x} + \mathbf{B}\mathbf{u} \tag{2.1}$$

$$\mathbf{y} = \mathbf{C}\mathbf{x} + \mathbf{D}\mathbf{u} \tag{2.2}$$

where $\mathbf{x}$ is the state vector, $\mathbf{u}$ the input vector and $\mathbf{y}$ the output vector. $\mathbf{A}$ is the system matrix, $\mathbf{B}$ the input matrix, $\mathbf{C}$ the output matrix and $\mathbf{D}$ the direct matrix.

If the input signals $u_1,\ldots, u_m$ of a system, have the Laplace transforms $U_1(s),\ldots, U_m(s)$ and the output signals $y_1,\ldots, y_p$ have the Laplace transforms $Y_1(s),\ldots, Y_p(s)$ they will be related as:

$$\begin{bmatrix} Y_1(s) \\ \cdots \\ Y_i(s) \\ \cdots \\ Y_p(s) \end{bmatrix} = \begin{bmatrix} G_{11}(s) & \ldots & G_{1j}(s) & \ldots & G_{1m}(s) \\ \cdots & \cdots & \cdots & \cdots & \cdots \\ G_{i1}(s) & \ldots & G_{ij}(s) & \ldots & G_{im}(s) \\ \cdots & \cdots & \cdots & \cdots & \cdots \\ G_{p1}(s) & \ldots & G_{pj}(s) & \ldots & G_{pm}(s) \end{bmatrix} \begin{bmatrix} U_1(s) \\ \cdots \\ U_j(s) \\ \cdots \\ U_m(s) \end{bmatrix} \tag{2.3}$$

Equation (2.3) can also be expressed as

$$\mathbf{Y}(s) = \mathbf{G}(s)\mathbf{U}(s) \tag{2.4}$$

where $\mathbf{G}(s)$ is a matrix containing the transfer functions of the system with $\mathbf{U}(s)$ as the input signal vector and $\mathbf{Y}(s)$ as the output signal vector.

The transfer function matrix $\mathbf{G}(s)$ can be determined by the relation

$$\mathbf{G}(s) = \mathbf{C}(s\mathbf{I} - \mathbf{A})^{-1}\mathbf{B} + \mathbf{D} \tag{2.5}$$

where $\mathbf{I}$ is the identity matrix.

$G_{ij}(s)$ is the transfer function with u_j as input and y_i as output:

$$G_{ij}(s) = K\frac{b(s)}{a(s)} \tag{2.6}$$

The denominator of $G_{ij}(s)$, $a(s)$, has an order of n, the number of states. The order of the numerator $b(s)$ is equal to or lower than n. The constant K can either be included in or excluded from $b(s)$. The roots of the expression $b(s) = 0$ which make $G_{ij}(S) = 0$, are referred to as zeros, and the roots of the expression $a(s) = 0$, which make the polynomial $G_{ij}(s) \rightarrow \infty$, are referred to as poles or eigenvalues. The equation $a(s)=0$ is also called the characteristic equation. For a given system, the poles are the same for all the transfer functions while the zeros differ from one transfer function to another. Knowing the location of the zeros and poles of a system, the system dynamics can be completely described.

2.1.1 Damping, eigenvalues, eigenfrequency, frequency and step response

Although the zeros influence the dynamics of a system, it is the poles which often play the most important role. With the knowledge of the pole location it is possible to determine the frequencies, where resonances can emerge, and if there is a risk for poor damping. When only the poles are investigated, they are usually referred to as eigenvalues, $\lambda_{1..n}$. With a denominator of order n, the impulse response, also called the natural response, of the transfer function (2.6) will be

$$h(t) = c_1 e^{\lambda_1} + ... + c_i e^{\lambda_i} + ... + c_n e^{\lambda_n} \tag{2.7}$$

The values of the constants $c_1...c_n$ depend on the location of both the zeros and poles. The eigenvalues can either be real, $\lambda_i = \sigma$, or complex, $\lambda_{i,\, i+1} = \sigma \pm j\omega$. A real eigenvalue gives a contribution to the natural response of

$$c_i e^{\lambda_i} = c_i e^{\sigma t} \tag{2.8}$$

and a complex eigenvalue pair gives a contribution of

$$c_i e^{\lambda_i} + c_i e^{\lambda_{i+1}} = \frac{c_i}{2} e^{\sigma t}(\cos \omega t) \tag{2.9}$$

From (2.8) and (2.9) it can be noted that with a positive real part of the eigenvalue the system will be negatively damped, i.e. unstable, and that with a negative, but small, real part the system will be poorly damped. If the eigenvalue has an imaginary part, the contribution to the natural response will be an oscillating term.

Consider a simple second-order system with the transfer function

$$H(s) = \frac{\omega_0^2}{s^2 + 2\xi\omega_0 s + \omega_0^2} \tag{2.10}$$

where ω_0 is the undamped natural angular frequency and ξ is the damping ratio.

The poles of the system are

$$P_{1,2} = -\xi\omega_0 \pm \omega_0\sqrt{1-\xi^2}. \tag{2.11}$$

In Fig. 2.1. the poles of the system with the damping ratio, ξ, being 0.1, 0.3 and 0.5 are presented.

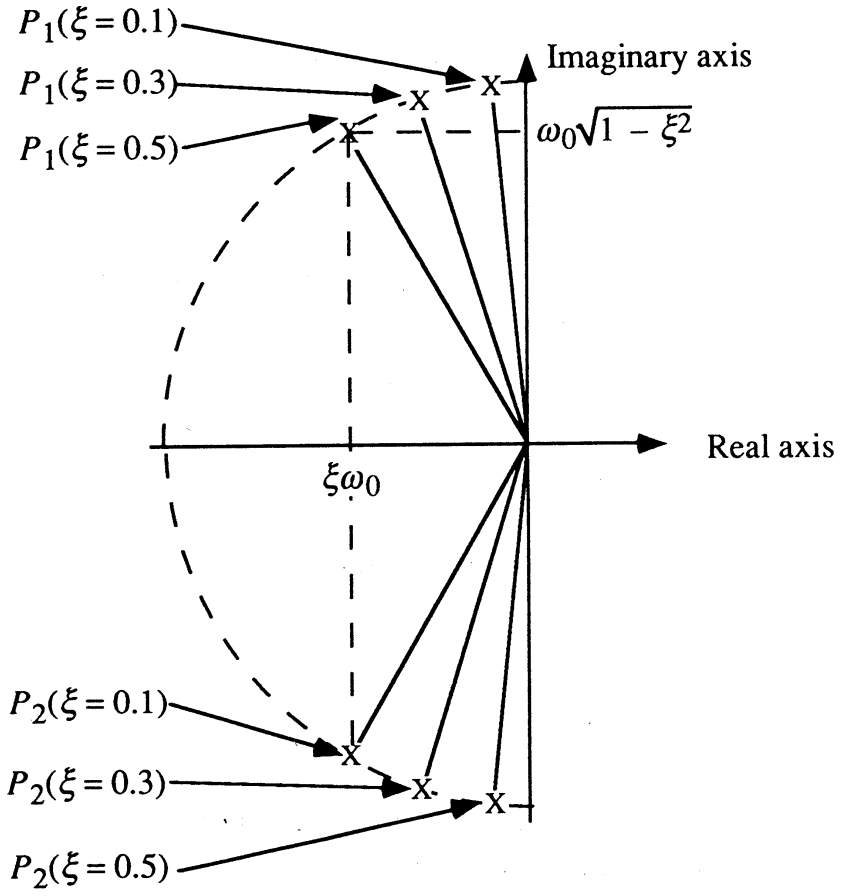

Figure 2.1. Location of poles in the S-plane with varied values of the damping ratio, ξ.

All poles have the same distance, ω_0, to the origin.

From the location of the poles (and zeros if there are any) the frequency response and the step response can be calculated as illustrated in Figs. 2.2 and 2.3, respectively.

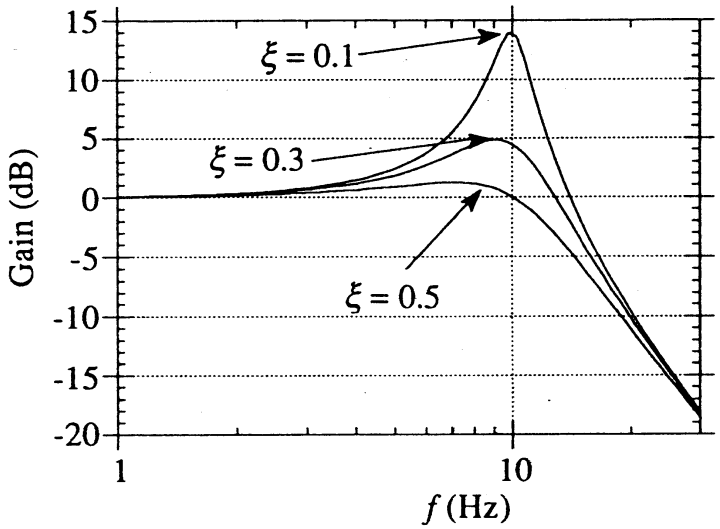

Figure 2.2. Gain of the transfer function H(s) with ω_0 = 100 and varied values of the damping ratio, ξ.

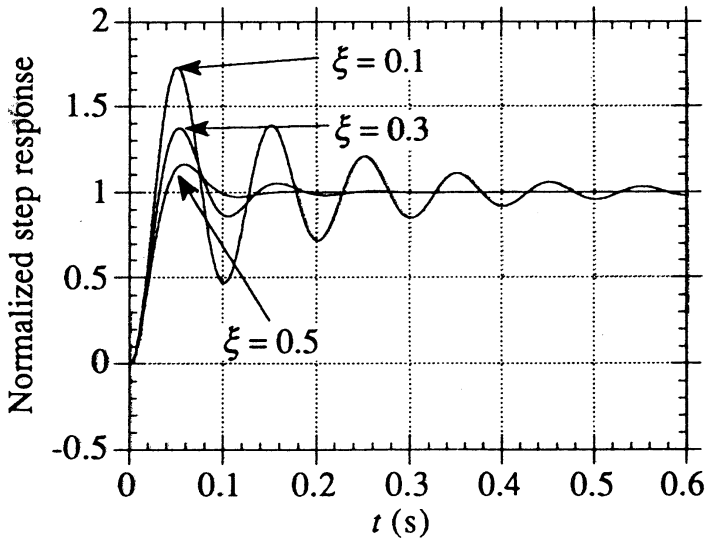

Figure 2.3. Step response of the transfer function H(s) with ω_0 = 100 and varied values of the damping ratio, ξ.

The reduced damping due to a small ξ is clearly visible in Figs. 2.2 and 2.3. If ξ is equal to $1/\sqrt{2}$, there will be no amplification in the frequency response for any frequency leading to a critically damped system and if $\xi>1$, the step response will not oscillate.

2.2 Equations of the three-phase induction machine

2.2.1 Generalized induction machine equations

When the induction machine dynamics is studied, some simplifying assumptions are usually made. The windings are considered to be sinusoidally distributed and the core losses are neglected. The machine parameters are considered to be constant, i.e. no change in the saturation level or influence of the skin effect. With these assumptions, the squirrel cage induction machine can be described by the following equations:

$$\underline{u}_s = \underline{i}_s R_s + \frac{d\underline{\Psi}_s}{dt} + j\omega_k \underline{\Psi}_s \tag{2.12}$$

$$0 = \underline{i}_r R_r + \frac{d\underline{\Psi}_r}{dt} + j(\omega_k - p\Omega_m)\underline{\Psi}_r \tag{2.13}$$

$$J_m \frac{d\Omega_m}{dt} = T_e - T_s \tag{2.14}$$

$$T_e = p\mathrm{Im}(\underline{\Psi}_s^* \underline{i}_s) \tag{2.15}$$

where $\underline{i}_s$, $\underline{i}_r$ are the stator and rotor current vectors, Ω_m is the mechanical rotor speed, ω_k the angular velocity of the coordinate system, T_s the shaft torque, T_e the electrodynamical torque and $\underline{u}_s$ the supply voltage vector. R_s, R_r are the stator and rotor resistances, J_m is the inertia of the machine and p the pole pair number. All the rotor parameters and variables are referred to the stator side. As can be noted from (2.15) the ratio between the numbers of turns in the two-phase winding and three-phase winding is chosen to be $\sqrt{2/3}$. The stator and rotor flux vectors are obtained by the following expressions:

$$\underline{\Psi}_s = L_s \underline{i}_s + L_m \underline{i}_r \tag{2.16}$$

$$\underline{\Psi}_r = L_r \underline{i}_r + L_m \underline{i}_s \tag{2.17}$$

L_s, L_r and L_m are the stator, rotor and magnetizing inductances, respectively. The system is non-linear as can be noted, if (2.16) or (2.17) is inserted to (2.15) or (2.13), respectively.

At $\omega_k=\omega_s$, the supply angular frequency, and with the voltage in the quadrature direction, the following system of induction machine equations is obtained with motor references:

$$\mathbf{U}=\mathbf{R}\,\mathbf{I}+\mathbf{L}\,\frac{d\mathbf{I}}{dt} \tag{2.18}$$

where **U** is the voltage vector, **I** is the current vector, **R** is the resistance matrix and **L** is the inductance matrix. The elements in the vectors and matrices are:

$$\mathbf{I}=\begin{bmatrix} i_{ds} \\ i_{dr} \\ i_{qr} \\ i_{qs} \\ \Omega_m \end{bmatrix} \quad \mathbf{U}=\begin{bmatrix} 0 \\ 0 \\ 0 \\ U_q \\ T_s \end{bmatrix} \quad \mathbf{L}=\begin{bmatrix} L_s & L_m & 0 & 0 & 0 \\ L_m & L_r & 0 & 0 & 0 \\ 0 & 0 & L_r & L_m & 0 \\ 0 & 0 & L_m & L_s & 0 \\ 0 & 0 & 0 & 0 & -J_m \end{bmatrix}$$

and

$$\mathbf{R}=\begin{bmatrix} R_s & 0 & -L_m\omega_s & -L_s\omega_s & 0 \\ 0 & R_r & L_r(p\Omega_m-\omega_s) & L_m(p\Omega_m-\omega_s) & 0 \\ L_m(\omega_s-p\Omega_m) & L_r(\omega_s-p\Omega_m) & R_r & 0 & 0 \\ L_s\omega_s & L_m\omega_s & 0 & R_s & 0 \\ 0 & 0 & -pL_m i_{ds} & pL_m i_{dr} & 0 \end{bmatrix}$$

where i_{ds}, i_{dr} i_{qr} and i_{qs} are the stator and rotor currents in direct and quadrature axes and U_q is the voltage in the quadrature axis. The induction machine model (2.18) will be referred to as the detailed model in this investigation.

Skin effect correction

With higher frequencies of the rotor currents, the value of the rotor resistance increases and the value of the rotor leakage inductance decreases due to the skin effect in the rotor conductors. At 40 Hz, the upper limit of investigation, the value of the rotor leakage inductance has approximately been reduced by 6 % while the rotor resistance value is 40 % higher than the dc-value. In this thesis the rotor leakage inductance is considered to be constant. By using a simple method the variation of the rotor resistance due to the skin effect in the rotor conductors is taken into account. One frequency of shaft torque disturbances is applied at each calculation and the value of the rotor resistance at this frequency is used. Another way of compensating for the skin effect proposed in [22] is to develop a layer model. By using this method the rotor conductors are transformed to a network of several thin conductors, leading to a large number of equations. The result from the method used is compared with results obtained by using a method based on superposition. A small-signal solution with adjusted values of the rotor resistance is added to a steady-state solution with the rotor resistance having its dc-value and it is found that the method used and the superposition method predicted similar results. The determination of the rotor resistance is presented in Appendix A.

2.2.2 The steady-state equivalent circuit of the induction machine

If the induction machine is operating in steady-state with a sinusoidal symmetrical supply voltage and the core losses are neglected, the machine can be described by the steady-state equivalent circuit, see Fig 2.4. All the parameters are referred to the stator side.

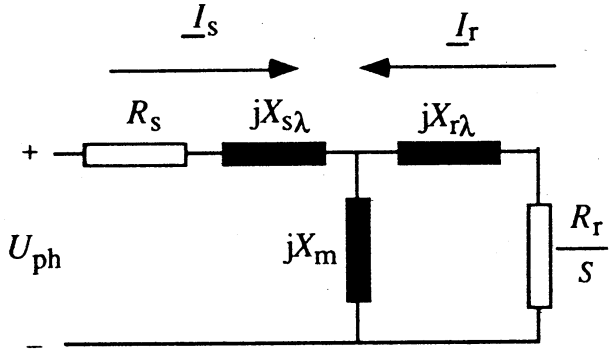

Figure 2.4. The steady-state equivalent circuit of the induction machine.

$X_{s\lambda}$, $X_{r\lambda}$ and X_m are the stator leakage, rotor leakage and magnetizing reactances respectively, S the slip and U_{ph} the phase voltage. $\underline{I}_s$ and $\underline{I}_r$ are the stator and rotor current phasors, respectively. The steady-state equivalent circuit can be simplified to a two-terminal network. In Fig 2.5 the simplified equivalent circuit is presented.

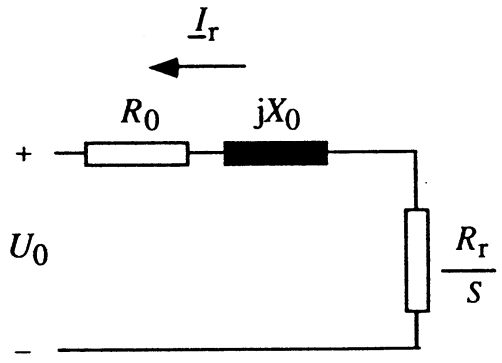

Figure 2.5. The simplified equivalent circuit of the induction machine.

The equivalent voltage, resistance and reactance are determined by the following equations:

$$U_0 = kU_{ph} \tag{2.19}$$

$$R_0 = kR_s \tag{2.20}$$

$$X_0 = X_{r\lambda} + kX_{s\lambda} \tag{2.21}$$

where

$$k = \frac{X_m}{X_m + X_{s\lambda}} \tag{2.22}$$

The electrodynamical torque, T_e, is in steady-state a function of the slip and can be determined by

$$T_e = \frac{3pR_r}{\omega_s S} \frac{U_0^2}{(R_0 + \frac{R_r}{S})^2 + X_0^2} \tag{2.23}$$

2.3 Application of linear theory on the induction machine equations.

If the induction machine equations are linearized at a certain operating-point, a small-perturbation state space model of the induction machine can be derived [23]. From this model, the small-perturbation transfer functions of the induction machine can be determined.

In this thesis there are six small-perturbation transfer functions of special interest. They are the transfer functions which can be derived with the disturbances in the shaft torque, amplitude and frequency of the supply voltage as inputs, and the disturbances in the rotor speed and electrodynamical torque as outputs, see Fig. 2.6.

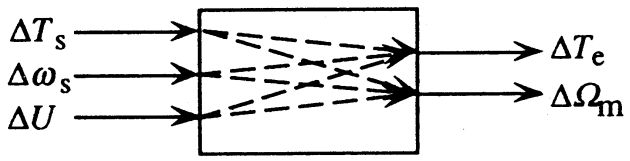

Figure 2.6. The induction machine as an input-output box.

Four induction machines are investigated. The parameters of the machines are presented in Table 2.1.

Table 2.1. Machine parameters for the investigated machines (cold machines). The rotor parameters are referred to the stator side.

Rated power P_n	2.4 MW	55 kW	22 kW	15 kW
Stator resistance, R_s	0.072 Ω	0.032 Ω	0.15 Ω	0.18 Ω
Rotor resistance, R_r	0.095 Ω	0.071 Ω	0.17 Ω	0.19 Ω
Stator leakage inductance, $L_{s\lambda}$	3.9 mH	0.52 mH	1.5 mH	2.2 mH
Rotor leakage inductance, $L_{r\lambda}$	7.1 mH	0.66 mH	1.7 mH	1.8 mH
Magnetizing inductance, L_m	204.8 mH	14.6 mH	38.5 mH	38.8 mH
Rated voltage, U_n	6000 V	380 V	380 V	380 V
Machine inertia, J_m	100 kgm^2	0.97 kgm^2	0.19 kgm^2	0.22 kgm^2
Number of pole pairs, p	4	4	4	6

The calculations are performed with the machines operating in rated generator operation with a supply frequency of 50 Hz. The supply voltage used for the larger machine is the rated voltage but for the three smaller machines the used voltage is 400 V. The reason for using 400 V instead of the rated voltage of 380 V, is that 400 V is the nominal grid voltage.

2.3.1 The eigenvalues of the induction machine

If the eigenvalues of the induction machine are determined, five eigenvalues will be obtained. It is not possible to solve the eigenvalues analytically, since there is no general solution to a fifth-order equation. However, if the rotor inertia is considered to be infinite (the mechanical equation (2.14) is removed), it will be possible to obtain analytical values on those four eigenvalues according to Narraway [24] and Policastro et al. [25]. In Table 2.2 the eigenvalues of the investigated machines are presented.

Table 2.2. The eigenvalues of the induction machines (rated generator operation).

	$\lambda_{1,2}$	$\lambda_{3,4}$	λ_5
2.4 MW machine	–6.8 ± j314	–4.60 ± j35	–8.1
55 kW machine	–27.3 ± j310	–30.8 ± j67	–59
22 kW machine	–50.0 ± j307	–23.6 ± j98	–52
15 kW machine	–47.2 ± j309	–19.5 ± j120	–46.2

From Table 2.2 it can be observed that the induction machine has two pairs of complex-conjugated eigenvalues and one real eigenvalue. This means that there are two eigenfrequencies: one upper, just below the supply angular frequency, 314 rad/s, 50 Hz, and one lower in the region of 35-120 rad/s, 5-20 Hz. A physical explanation of the two eigenfrequencies is given by Lorenzen [26]. The upper resonance exists due to the oscillation in the magnetic energy between the rotor and the stator and the lower eigenfrequency indicates the possibility of energy oscillations between the kinetic energy stored in the rotor and the magnetic energy stored in the leakage fields of the machine.

2.3.2 Small-perturbation transfer functions of the induction machine

The small-perturbation transfer functions presented in this Section will be determined for the 15 kW machine. The results from calculations performed on the other machines are mainly the same but the damping ratios and eigenfrequencies are of course different for different machines. The small-perturbation transfer function with the shaft torque as input and the electrodynamical torque as output is for the 15 kW machine operating with rated torque as generator:

$$\frac{\Delta T_e}{\Delta T_s} = \frac{14785\,(s^2 + 47.0\,s + 97025)\,(s + 46.2)}{(s^2 + 39.0\,s + 14727)\,(s + 94.5\,s + 97388)\,(s + 46.2)} \qquad (2.24)$$

The gain of the transfer function (2.24) is presented in Fig. 2.7.

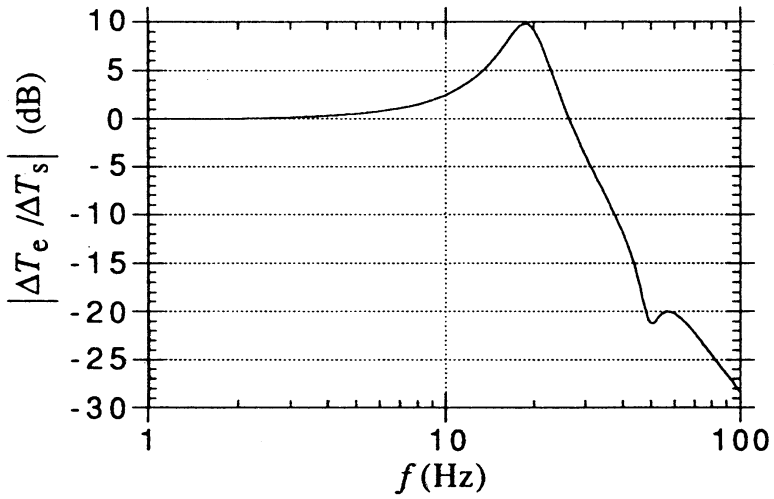

Figure 2.7. Gain of the transfer function $\Delta T_e/\Delta T_s$.

From (2.24) and Fig. 2.7 it can be observed that the linearized transfer function $\Delta T_e/\Delta T_s$ acts as a second-order low-pass filter with a resonance frequency around 18 Hz caused by the lower eigenfrequency, often referred to as the dominating one. The amplification from the disturbance in shaft torque to the disturbance in electrodynamical torque at 18 Hz is almost three times compared to the low-frequency case. The upper eigenfrequency is suppressed by the complex zero pair in (2.24). In fact, the effect of the double zero is that the damping of $\Delta T_e/\Delta T_s$ is improved around the disturbance frequency of 50 Hz which can be seen in Fig. 2.7. The real pole and the real zero also almost have the same location. If the three zeros cancel out the three poles, a second-order system will be obtained:

$$\frac{\Delta T_e}{\Delta T_s} \approx \frac{14727}{(s^2 + 39.0s + 14727)} = \frac{\omega_0^2}{s^2 + 2\xi\omega_0 s + \omega_0^2} \qquad (2.25)$$

With the 15 kW machine, the undamped dominating eigenfrequency

$$f_0 = \frac{\omega_0}{2\pi} \tag{2.26}$$

is situated at 19 Hz with a damping ratio of ξ = 0.16. The undamped eigenfrequency will from now on be referred to as the eigenfrequency only. In Table 2.3 the dominating eigenfrequencies and the damping at these eigenfrequencies are presented for the investigated machines.

Table 2.3. Location of and damping at the dominating eigenfrequency for the investigated machines (rated generator operation).

	f_0 (Hz)	ξ
2.4 MW machine	5.6	0.13
55 kW machine	12	0.42
22 kW machine	16	0.23
15 kW machine	19	0.16

In Fig. 2.8 the gain of the transfer function (2.25) is compared with the gain of the transfer function (2.24).

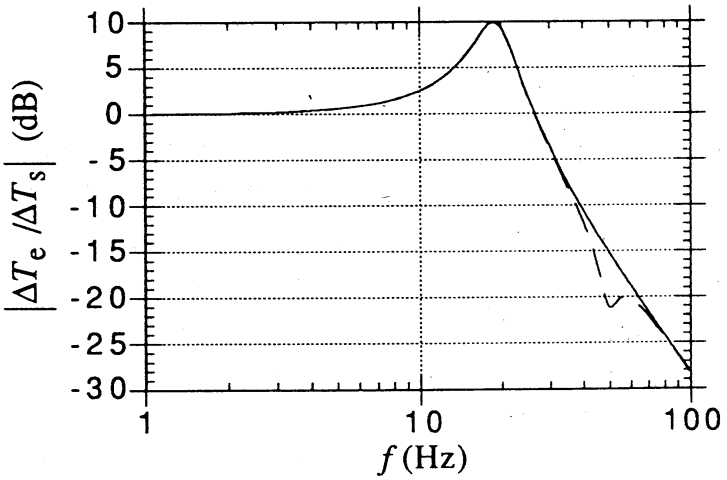

Figure 2.8. Gain of the transfer function $\Delta T_e/\Delta T_s$. The dashed line represents calculations performed with the detailed model and the solid line represents calculations performed using the simplified transfer function.

As can be seen in Fig. 2.8, the gain of the transfer function $\Delta T_e/\Delta T_s$ predicted using the detailed transfer function and the simplified one are almost identical. The only notable difference is around a disturbance frequency of 50 Hz, where the effect of the neglected upper double pole and double zero is visible.

With the disturbance in the rotor speed as output and the disturbance in the shaft torque as input the small-perturbation transfer function will be

$$\frac{\Delta\Omega_m}{\Delta T_s} = \frac{-4.54\,(s^2 + 92.6\,s + 2142)\,(s^2 + 87.2\,s + 96960)}{(s^2 + 39\,s + 14727)\,(s^2 + 94.5\,s + 97388)\,(s + 46.2)} \qquad (2.27)$$

The gain of the transfer function $\Delta\Omega_m/\Delta T_s$ is presented in Fig 2.9.

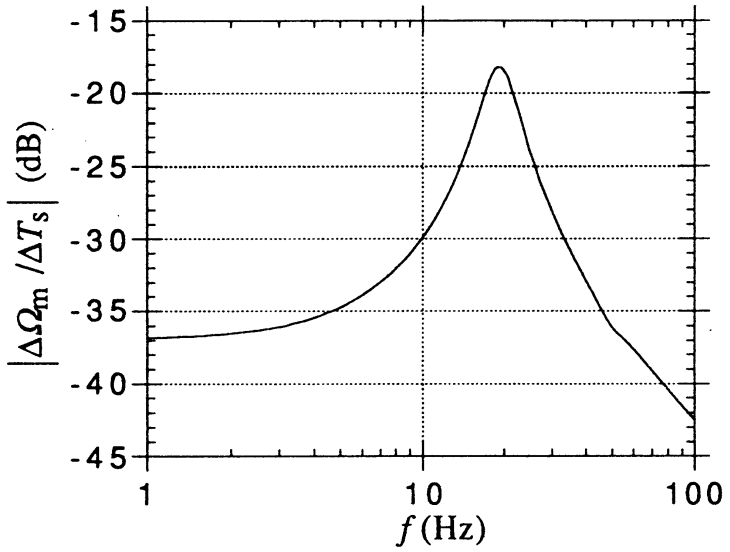

Figure 2.9. Gain of the transfer function $\Delta\Omega_m/\Delta T_s$.

The DC-gain is –37 dB which corresponds to the slope of the steady-state torque speed curve at rated operating-point as a generator. The amplification at the lower, dominating, eigenfrequency is as high as 7 times compared to the low-frequency case. Again the effect of the upper pole pair is eliminated by the upper zero pair and the real pole has a location close to one of the zeros. If these three zeros cancel out three of the poles, a second-order system will be obtained:

$$\frac{\Delta\Omega_m}{\Delta T_s} \approx \frac{-1}{J_m}\frac{(s + 46.3)}{(s^2 + 39.0\,s + 14727)} = \frac{-1}{J_m}\frac{(s + A)}{s^2 + 2\xi\omega_0 s + \omega_0^2} \qquad (2.28)$$

In Fig. 2.10 the simplified small-perturbation transfer function $\Delta\Omega_m/\Delta T_s$ is compared with the detailed one.

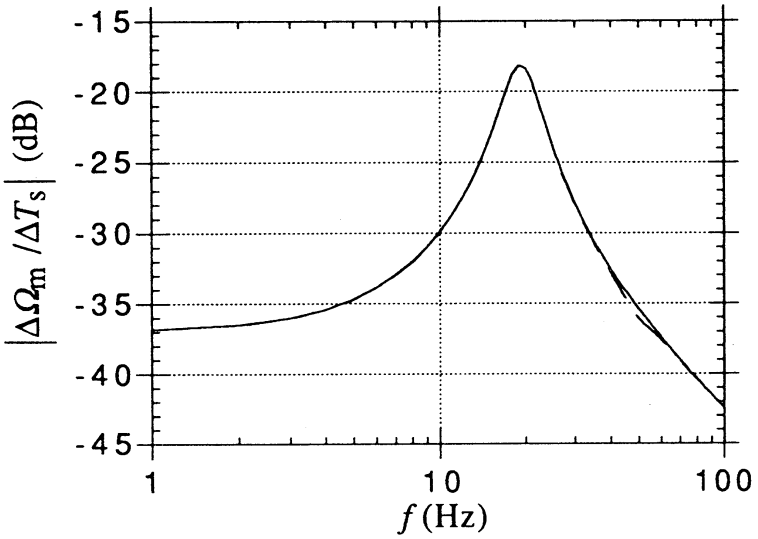

Figure 2.10. Gain of the transfer function $\Delta\Omega_m/\Delta T_s$. The dashed line represents calculations performed using the detailed model and the solid line represents calculations performed using the simplified transfer function.

In Fig. 2.10 it can be observed that the agreement between the predictions of the gain obtained by using (2.27) and (2.28) is very good. The parameters A, ω_0 and ξ of these linear second-order transfer functions depend on the operating-point. In Table 2.4 the parameters are presented for some different operating-points of the 15 kW machine.

Table 2.4. Parameters of the second-order numerical transfer functions for some different operating-points of the 15 kW machine.

Torque	ω_0	ξ	A
T_n (mot)	118.0	0.170	46.3
$T_n/4$ (mot)	120.2	0.161	46.3
No-load	120.6	0.159	46.3
$T_n/4$ (gen)	121.0	0.158	46.3
T_n (gen)	121.3	0.161	46.3

From Table 2.4 it can be observed that the damping increases some when the machine is loaded, especially in motor operation, while the undamped angular frequency almost remains unchanged.

The gain of the small-perturbation transfer function with the supply voltage as input and the electrodynamical torque as output

$$\frac{\Delta T_e}{\Delta U} = \frac{835.8\, s\,(s + 55.2)\,(s + 50.8)\,(s - 63.5)}{(s^2 + 39.0\, s + 14727)\,(s^2 + 94.5\, s + 97388)\,(s + 46.2)} \qquad (2.29)$$

is presented in Fig 2.11.

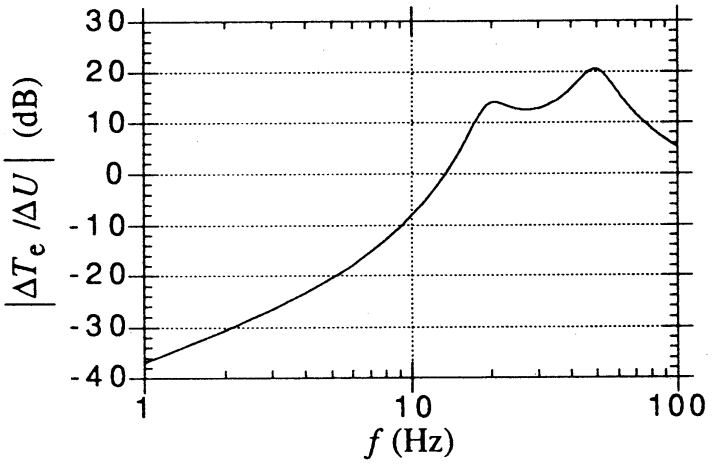

Figure 2.11. Gain of the transfer function $\Delta T_e/\Delta U$.

Both eigenfrequencies are visible in this case making it impossible to simplify (2.29) to a second-order model with an acceptable loss of accuracy by neglecting the effect of the upper eigenfrequency.

The small-perturbation transfer function with the rotor speed as output

$$\frac{\Delta \Omega_m}{\Delta U} = \frac{3800\,(s + 55.2)\,(s + 50.8)\,(s - 63.5)}{(s^2 + 39.0\, s + 14727)\,(s^2 + 94.5\, s + 97388)\,(s + 46.2)} \qquad (2.30)$$

can also be obtained by applying small-signal analysis on (2.14) which gives

$$\frac{\Delta \Omega_m}{\Delta U} = \frac{\Delta T_e}{\Delta U} \frac{1}{J_m\, s} \qquad (2.31)$$

and inserting (2.29) into (2.31) since the shaft torque is constant.

It is interesting to note that the transfer functions (2.29) and (2.30) are mixed phase systems. This matter can be studied more in detail in [27] but the consequence for the induction machine will be dealt with in Section 5.4.2. The gain of the transfer function (2.30) is presented in Fig. 2.12.

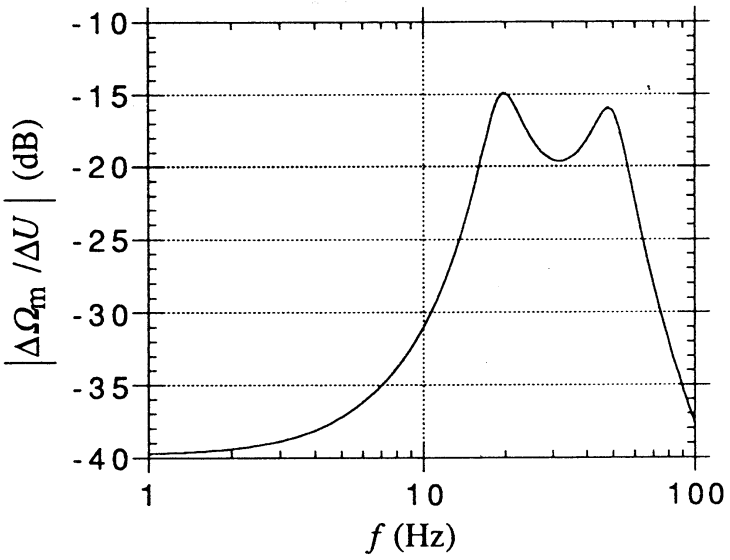

Figure 2.12. Gain of the transfer function $\Delta\Omega_m/\Delta U$.

Finally, the transfer functions with the frequency of the supply voltage as input

$$\frac{\Delta T_e}{\Delta \omega_s} = \frac{49437\, s\,(s + 46.2)\,(s + 2210)}{(s^2 + 39.0\, s + 14727)\,(s^2 + 94.5\, s + 97388)\,(s + 46.2)} \qquad (2.32)$$

and

$$\frac{\Delta \Omega_m}{\Delta \omega_s} = \frac{224720\,(s + 46.2)\,(s + 2210)}{(s^2 + 39.0\, s + 14727)\,(s^2 + 94.5\, s + 97388)\,(s + 46.2)} \qquad (2.33)$$

have the gains presented in Figs. 2.13 and 2.14.

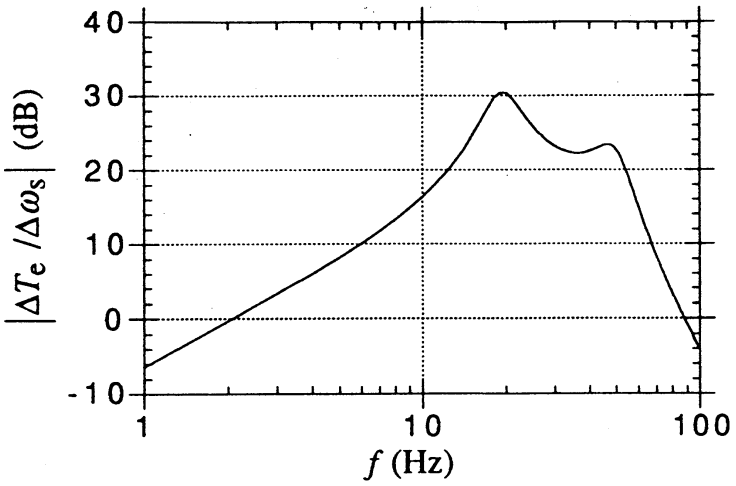

Figure 2.13. Gain of the transfer function $\Delta T_e/\Delta\omega_s$.

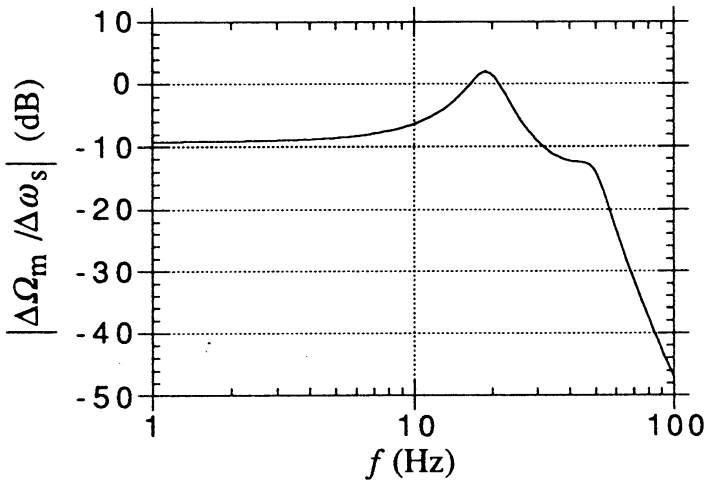

Figure 2.14. Gain of the transfer function $\Delta\Omega_m/\Delta\omega_s$.

Also in this case, the transfer function with the rotor speed variation as output can be derived from the transfer function with the electrodynamical torque variation as output inserted into (2.31). The lower eigenfrequency is of more importance than the higher one for the frequency transfer functions. However, the influence of the higher eigenfrequency can not be neglected without a larger loss of accuracy as in the case with the disturbance in the shaft torque as input, but still, it is of less importance than in the case with the disturbance in the amplitude of the supply voltage as input.

2.3.3 First-order models of the induction machine

The slope of the steady-state torque speed curve can be determined by a differentiation of (2.23) with respect to the slip:

$$\frac{dT_e}{ds} = \frac{6pU_0^2R_r^2\,(R_0 + \frac{R_r}{S}) - 3pU_0^2R_rS}{S^3\omega_s((R_0 + \frac{R_r}{S})^2 + (X_0 + X_{r\lambda})^2)^2} \tag{2.34}$$

At the synchronous speed, $S = 0$, (2.34) can be simplified to:

$$\frac{dT_e}{dS} = \frac{3pU_0^2}{\omega_s R_r} \tag{2.35}$$

From (2.35), the linearized torque-speed characteristic at the synchronous speed is obtained:

$$\Delta T_e = \frac{3pU_0^2}{\omega_s R_r}\Delta S = -\frac{3pU_0^2}{\omega_s^2 R_r}\Delta\Omega_m \tag{2.36}$$

In Fig. 2.15. the linearized torque speed characteristic (2.36) is compared with the steady-state torque speed characteristic obtained by using (2.23).

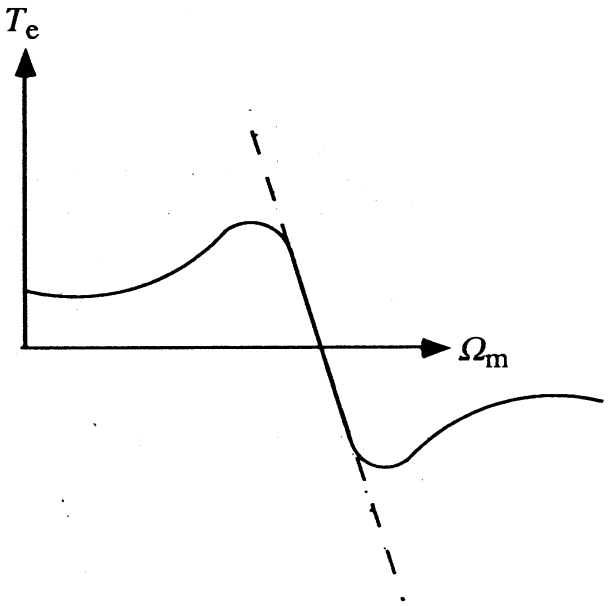

Figure 2.15. Comparison between linearized (dashed line) and non-linear (solid line) torque-speed characteristics.

The steady-state torque speed error grows as the slip increases, especially in motor operation. In Table 2.5 the steady-state error is presented for the induction machines operating at rated torque in motor as well as in generator operation.

Table 2.5. Steady-state slip error at rated torque, T_n.

	2.4 MW	55 kW	22 kW	15 kW
Motor	–8.1 %	–4.4 %	–7.2 %	–6.1 %
Generator	–5.3 %	–0.4 %	–1.9 %	–1.1 %

If (2.14) is Laplacetransformed and small-signal analysis is applied we get:

$$J_m s \Delta\Omega_m = \Delta T_e - \Delta T_s \tag{2.37}$$

By inserting (2.36) into (2.37) the damper model, a linear first-order model of the induction machine is obtained:

$$H(s) = \frac{\Delta T_e}{\Delta T_s} = \frac{1}{1 + s\dfrac{\omega_s^2 J_m R_r}{3p^2 U_0^2}} \tag{2.38}$$

In Fig. 2.16 a mechanical analogy of the damper model is presented:

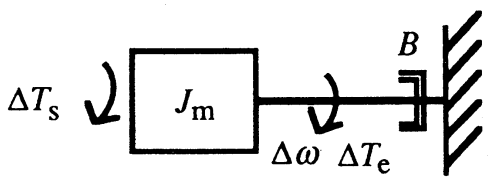

B=Equivalent damper

Figure 2.16. Mechanical analogy of the damper model.

If (2.23) is inserted into (2.37) instead, we will receive a first-order non-linear model. In this model the value of the damper B varies as the operating-point changes.

2.3.4 Simplified analysis by neglecting the stator resistance

If the stator resistance is neglected, it will be possible to derive analytical second-order transfer functions of the induction machine operating at no-load with the shaft torque as input according to Kovacs [18]:

$$\frac{\Delta T_e}{\Delta T_s} = \frac{(\frac{L_m}{L_s})^2 \frac{p^2 \Psi_{ds}^2}{J_m L_r'}}{s^2 + s\frac{R_r}{L_r'} + (\frac{L_m}{L_s})^2 \frac{p^2 \Psi_{ds}^2}{J_m L_r'}} \tag{2.39}$$

$$\frac{\Delta \Omega_m}{\Delta T_s} = \frac{\frac{-1}{J_m}(s + \frac{R_r}{L_r'})}{s^2 + s\frac{R_r}{L_r'} + (\frac{L_m}{L_s})^2 \frac{p^2 \Psi_{ds}^2}{J_m L_r'}} \tag{2.40}$$

where

$$L_r' = L_{s\lambda}\frac{L_m}{L_s} + L_{r\lambda} \tag{2.41}$$

is the rotor transient inductance and

$$\Psi_{ds} = \frac{U_q}{\omega_s} \tag{2.42}$$

is the d-component of the stator flux. L_r' is also presented in Fig 2.17.

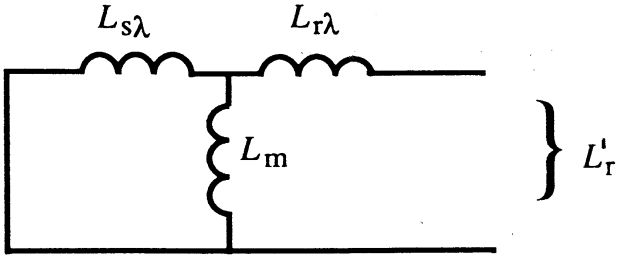

Figure 2.17. Rotor transient inductance.

Analogously the stator transient inductance can be derived:

$$L_s' = L_{r\lambda}\frac{L_m}{L_r} + L_{s\lambda} \tag{2.43}$$

In Fig. 2.18 the stator transient inductance is presented.

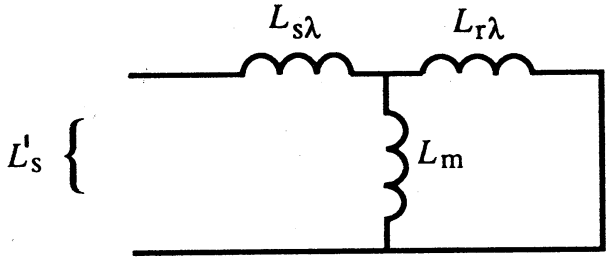

Figure 2.18. Stator transient inductance.

The induction machine can now be represented by the mechanical and electrical analogies presented in Fig. 2.19 [4, 18].

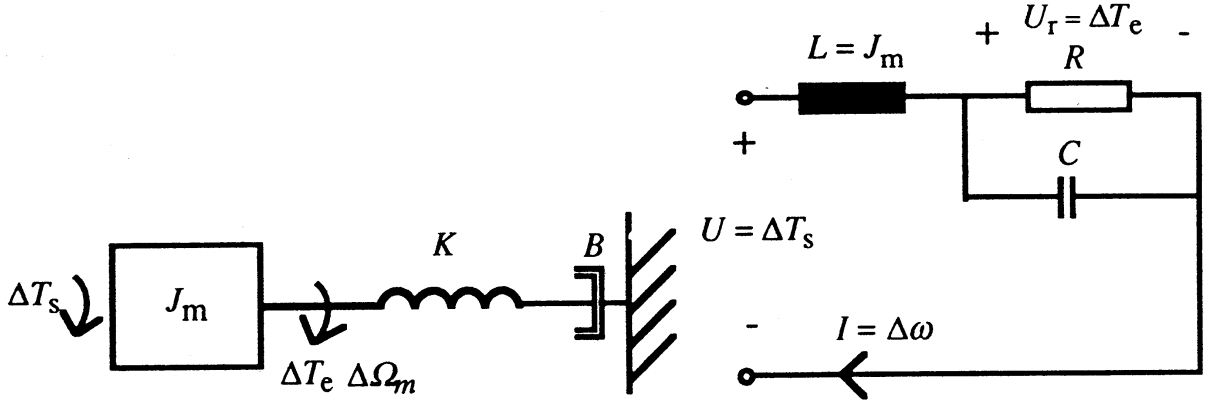

Figure 2.19. Mechanical and electrical second-order models of the induction machine.

The values of the equivalent spring constant, damper, capacitor and resistance are:

$$K = \left(\frac{L_m}{L_s}\right)^2 \frac{p^2 \psi_{ds}^2}{L'_r} \tag{2.44}$$

$$B = \left(\frac{L_m}{L_s}\right)^2 \frac{p^2 \psi_{ds}^2}{R_r} \tag{2.45}$$

$$C = \left(\frac{L_s}{L_m}\right)^2 \frac{L'_r}{p^2 \psi_{ds}^2} \tag{2.46}$$

$$R = \left(\frac{L_m}{L_s}\right)^2 \frac{p^2 \psi_{ds}^2}{R_r} \tag{2.47}$$

With numerical values for the 15 kW machine inserted into (2.39) and (2.40) the damping ratio is $\xi = 0.191$ and the undamped angular frequency $\omega_0 = 120.7$. If these values are compared with the values presented in Table 2.4 it can be noted that the largest error when neglecting the stator resistance is that the damping at the dominating eigenfrequency is overestimated.

It is also possible to use these Neglecting Stator Resistance-models (NSR-models) to determine the response to disturbances in the supply frequency. The electrical and mechanical models from Fig 2.19 can now be modified as in Fig. 2.20.

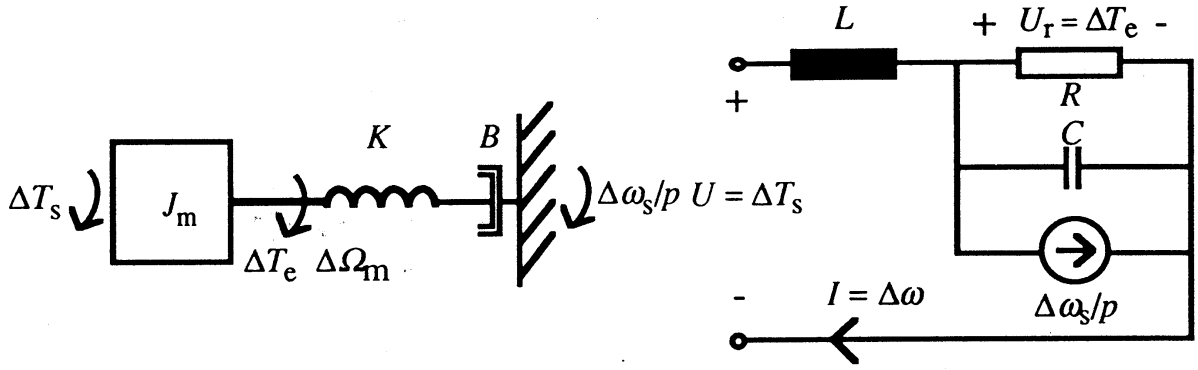

Figure 2.20. Simplified models (NSR-models) of the induction machine to determine the response to disturbances in the supply frequency and shaft torque.

The transfer functions with the supply frequency as input can now be derived from Fig. 2.20:

$$\frac{\Delta T_e}{\Delta \omega_s} = \frac{s\left(\frac{L_m}{L_s}\right)^2 \frac{p\Psi_{ds}^2}{L_r'}}{s^2 + s\frac{R_r}{L_r'} + \left(\frac{L_m}{L_s}\right)^2 \frac{p^2\Psi_{ds}^2}{J_m L_r'}} \tag{2.48}$$

$$\frac{\Delta \Omega_m}{\Delta \omega_s} = \frac{\left(\frac{L_m}{L_s}\right)^2 \frac{p\Psi_{ds}^2}{J_m L_r'}}{s^2 + s\frac{R_r}{L_r'} + \left(\frac{L_m}{L_s}\right)^2 \frac{p^2\Psi_{ds}^2}{J_m L_r'}} \tag{2.49}$$

This approach to derive simplified transfer functions cannot be used to derive models with the amplitude of the supply voltage as input.

3 MEASUREMENT PROCEDURE

The measurements are made on the 15 kW induction machine. A converter-controlled dc-machine is used to create torque variations on the shaft of the induction machines. The rotor speed and electric power response are together with the shaft torque measured into a computer. The experimental set-up is presented in Fig. 3.1.

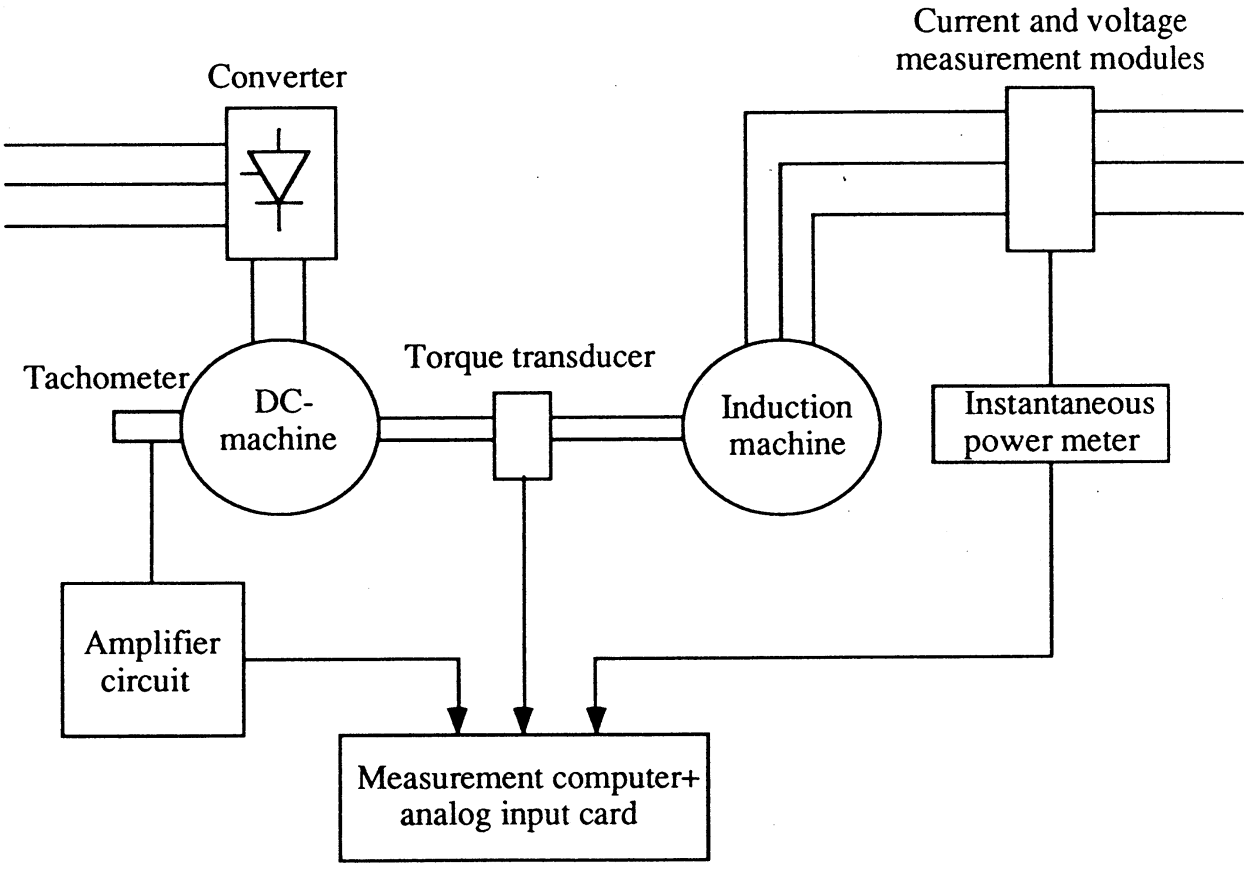

Figure 3.1. The experimental set-up.

The experimental equipment used in the dynamic measurements is presented in Table 3.1.

Table 3.1. The experimental and measurement equipment.

torque transducer	HBM T30FN, 500 Nm
current modules	LEM (Liasons Électroniques Mécaniques) LT 100 S
voltage modules	LEM (Liasons Électroniques Mécaniques) LV 100
analog input card	National Instruments NB-MIO-16
induction machine	ABB MBT-180L, 15 kW, 970 rpm
direct current machine	ABB DMP-4 S, 40.1 kW, 2470 rpm
converter	ABB TYRAK S 120 A
tachometer	Radio-energie, Dynamo Tachometer REo 444 R1

The electrical power P_e is calculated from the voltages and currents measured by an instantaneous power meter consisting of analog multipliers, AD 632, and a summing amplifier based on an operational amplifier, LF 347. The instantaneous power meter is presented in Fig. 3.2.

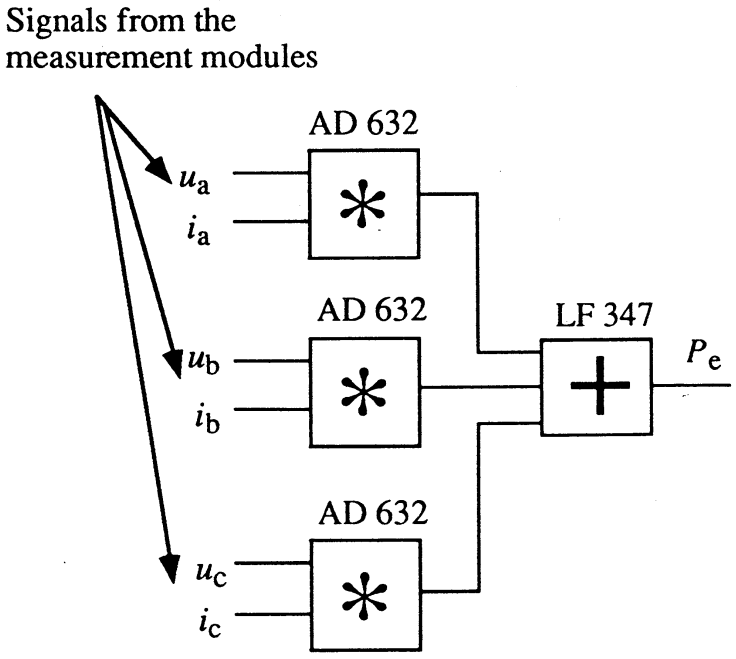

Figure 3.2. Instantaneous power meter.

The reason for using this type of power meter, is that conventional power meters have too a low bandwidth.

Knowing the air gap power, P_δ, the electrodynamical torque T_e can be determined:

$$T_e = p\frac{P_\delta}{\omega_s} \tag{3.1}$$

The air gap power can be calculated from the electric power and the stator losses:

$$P_\delta = P_e - P_{Cus} - P_{Fes} \tag{3.2}$$

where P_{Cus} represents the stator resistance losses and P_{Fes} represents the stator core losses. The stator resistance losses can be calculated from the stator currents:

$$P_{Cus} = R_s i_a^2 + R_s i_b^2 + R_s i_c^2 \tag{3.3}$$

With the stator core losses, P_{Fes}, regarded as constant, the electrodynamical torque, T_e, can now be determined:

$$T_e = p\frac{P_e - P_{Cus} - P_{Fes}}{\omega_s} \tag{3.4}$$

Linear systems can be identified when knowing the input and the output signals [28]. Here, the input signal is the shaft torque and the output signals are the rotor speed and electrodynamical torque. One suitable method is the PRBS (Pseudo-Random Binary Signal) which is an input signal varying between two levels with a suitable frequency spectrum. It is not possible to receive a shaft torque which varies between two levels, so this method has to be somewhat modified. The desired frequency region is also well-known, making it possible to use a square-wave signal with a constant frequency of 2 Hz. The torque reference signal is presented together with the created shaft torque pulsations in Fig. 3.3.

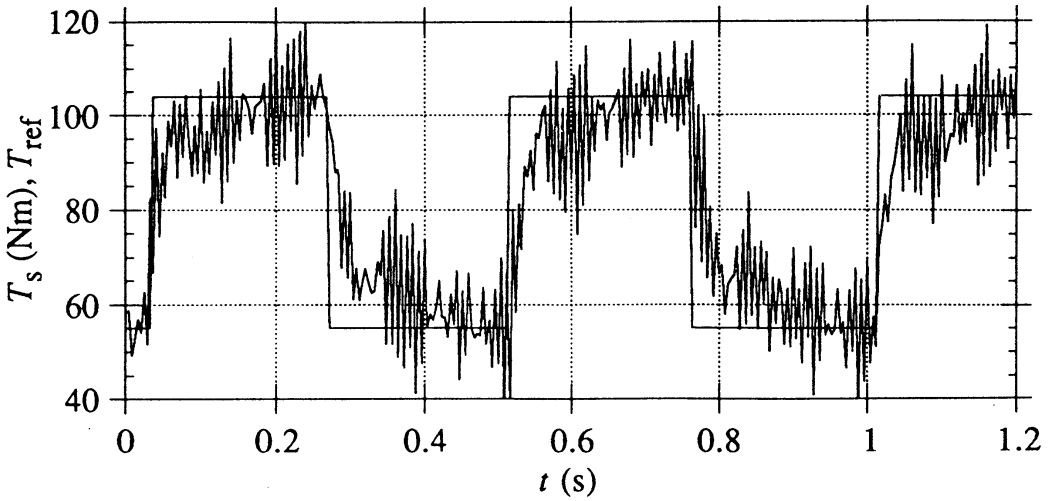

Figure 3.3. The reference signal to the rectifier and the measured shaft torque.

The torque pulsations create electrical power pulsations as shown in Fig. 3.4.

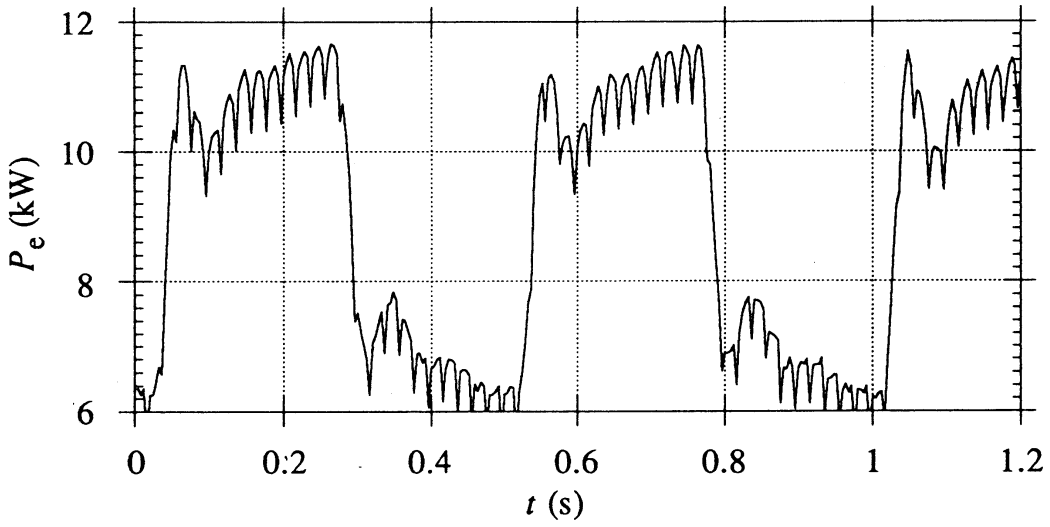

Figure 3.4. The measured electrical power.

Knowing the input and output signals, a suitable model is constructed. The use of this model is somewhat limited, because it is only valid for a small disturbance around a specific operating-point. But the dominant eigenvalues predicted by this method match well the result obtained by the safer method of sinusoidal pendulums. The advantage with the PRBS-method is that it needs a very short measurement time. A few seconds are enough to identify the dominant eigenvalues. The oscillation observed in Fig. 3.3 is a mechanical oscillation originating from the measurement set-up with a frequency of 130 Hz. In Fig. 3.4 the dominating disturbance frequency is 50 Hz. This is one of the reasons why 40 Hz is selected to be the upper limit for investigation.

The system identification methods require a linear system. In order to observe non-linearities a more time-consuming method is used. Sinusoidal-shaped torque pulsations on the machine shaft are obtained by controlling the rectifier in this way. The rotor speed and electrical power are measured and the electrodynamical torque is calculated. Since the measured signals, especially the rotor shaft torque and rotor speed signal, contain a considerable amount of noise, the measured signals have to be frequency-analysed. The ratios and phase shifts are determined at 15 frequency points, from 1 Hz up to 40 Hz. In each case 8192 values are collected per channel, with a sample rate of 20 times higher than the applied disturbance frequency in order to obtain as high an accuracy as possible. One example of a measurement "shot" is presented in Fig. 3.5.

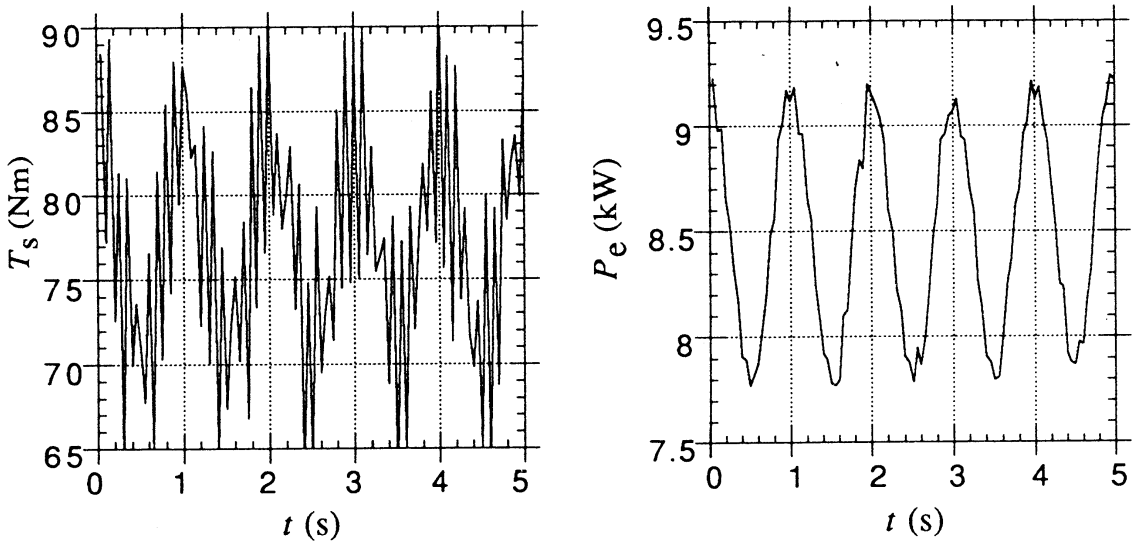

Figure 3.5. Example of measurements with sinusoidal pendulums.

4 COMPARISON BETWEEN DIFFERENT MODELS AND MEASUREMENTS

4.1 Torque pulsation

The measurements and calculations presented in this Section are made on the 15 kW machine operating as a generator with a driving shaft torque of 43 Nm (0.34 times the rated torque). The amplitude of the shaft torque pulsations, ΔT_s, is approximately 4 Nm and the frequency of the perturbations are varied from 1 Hz up to 40 Hz. The models used to determine the response to pulsations in the shaft torque are presented in Table 4.1.

Table 4.1. Models used to determine the response to pulsations in the shaft torque.

Model	Abbreviation	Equation(s)
Detailed model	Det-model	(2.18)
Small-perturbation model	SP-model	(2.24) and (2.27)
Neglecting stator resistance model	NSR-model	(2.39) and (2.40)
Linear damper model	LD-mod	(2.38)

The results from the second-order numerical models are not presented here, since the results predicted with these models are almost the same as the results obtained by using the small-perturbation models for frequencies below 40 Hz. The models are temperature-corrected, the detailed model is also corrected for the skin effect in the rotor conductors. After each completed measurement the machine is stopped and disconnected from the grid making it possible to measure the stator resistance. The rotor resistance value is obtained by measuring the slip and using (2.36). The measured and calculated gains and phase shifts of the transfer functions $\Delta T_e/\Delta T_s$ and $\Delta \Omega_m/\Delta T_s$ are presented in Figs. 4.1-4.4.

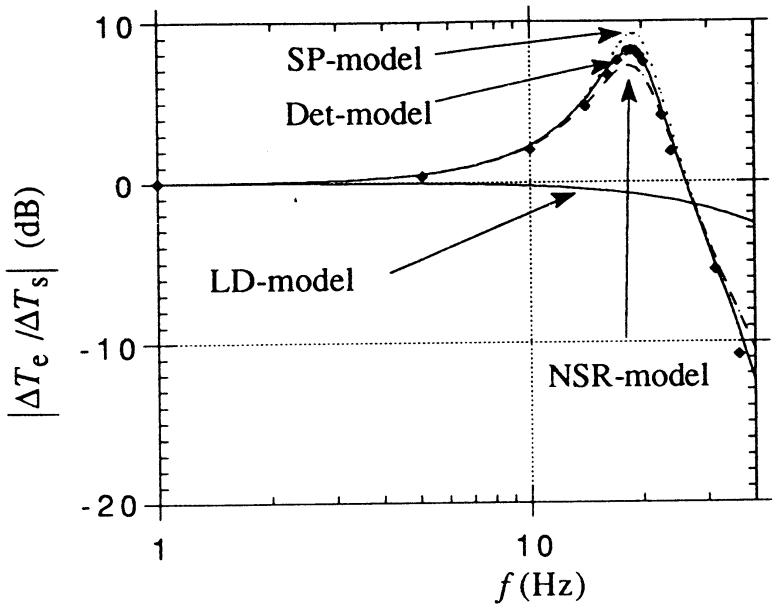

Figure 4.1. Gain of the transfer function $\Delta T_e/\Delta T_s$. The dots are measured values and the lines are values determined by means of the different models.

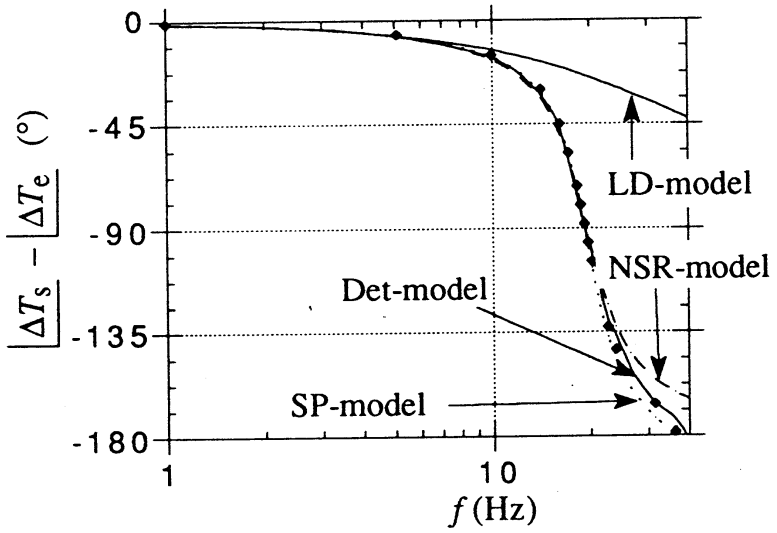

Figure 4.2. Phase shift of the transfer function $\Delta T_e/\Delta T_s$. Lines and dots as in Fig 4.1.

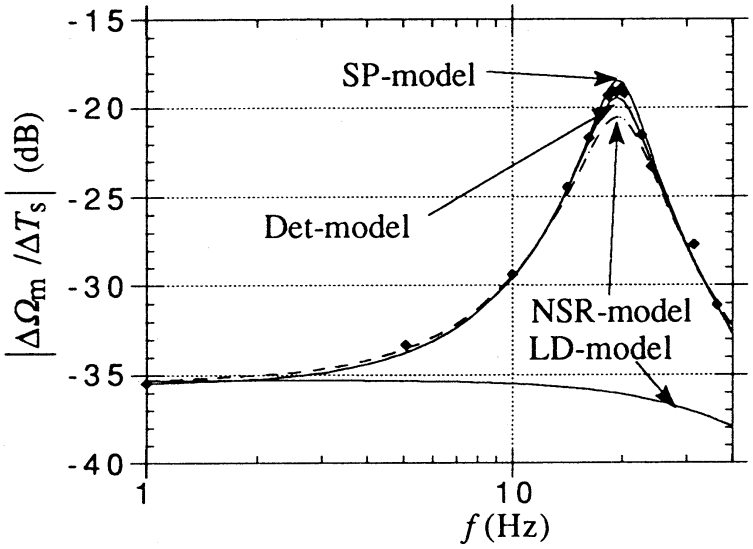

Figure 4.3. Gain of the transfer function $\Delta\Omega_m/\Delta T_s$. Lines and dots as in Fig 4.1.

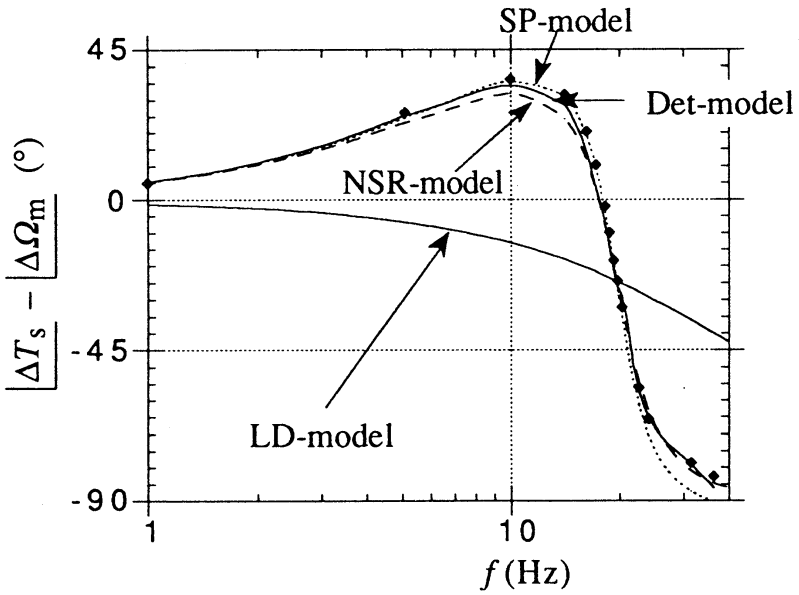

Figure 4.4. Phase shift of the transfer function $\Delta\Omega_m/\Delta T_s$. Lines and dots as in Fig 4.1.

The measured values of the gain and phase shift of the transfer function $\Delta T_e/\Delta T_s$ agree well with the values predicted using the detailed model. When predicting the gain and phase shift of the transfer functions $\Delta\Omega_m/\Delta T_s$ using the detailed model, the damping is somewhat overestimated. The reason for this is not further investigated, since the errors are within the accuracy desired. The results obtained using the small-perturbation models underestimate the damping due to the fact that these models do not take the skin effect into account. The NSR-

model overestimate the damping as mentioned in Section 2.3.4. The damper model can only be used to calculate the response to very low-frequency perturbations and the error towards the values predicted with the detailed model is presented in Table 4.2.

Table 4.2. Discrepancy in the prediction of the gain and phase shift between the detailed model and the damper model at some frequencies.

f (Hz)	Gain discrepancy of $\Delta T_e/\Delta T_s$ (dB)	Gain discrepancy of $\Delta\Omega_m/\Delta T_s$ (dB)	Phase discrepancy of $\Delta T_e/\Delta T_s$ (°)	Phase discrepancy of $\Delta\Omega_m/\Delta T_s$ (°)
1	0 (0 %)	0 (0 %)	–0.1	7
3	–0.20 (–2.4%)	–0.6 (–7 %)	–0.3	20
5	–0.60 (–7.1%)	–1.77 (–23%)	–0.7	32
10	–2.52 (–34 %)	–6.1 (–101 %)	–3.6	47

The negligence of the stator resistance in the NSR-model and the damper model gives an error which can be seen in Fig. 4.3, where the two models over-estimated the gain of the transfer function $\Delta\Omega_m/\Delta T_s$ for very low-frequency perturbations. In this case, the operating-point is close to the no-load point and the error is small. However, with an operating-point closer to the stall-point, the error will be larger, see Table 2.5, and it may be necessary to use the non-linear damper model instead.

The damper model can be used below a frequency limit, which depends on the accuracy desired and the purpose of the investigation. If, for instance, the criteria is to have a gain error of the transfer function $\Delta T_e/\Delta T_s$ less than 3 %, the frequency limit, f_l, where to choose between the damper model and the detailed model will be 3 Hz. The limit frequencies for the investigated machines, with this criteria, are presented in Table 4.3 together with the dominating eigenfrequencies.

Table 4.3. The dominating eigenfrequencies and suggested limit frequencies for the damper model.

	f_0 (Hz)	f_l (Hz)
15 kW machine	19	3
22 kW machine	16	3
55 kW machine	12	2.5
2.4 MW machine	5.6	1.0

From Table 4.3 it can be observed that the limit frequency in this case is approximately one fifth of the dominating eigenfrequency of the machine. So the validity of the damper model for a given accuracy can approximately be expressed as a certain part of the eigenfrequency.

One interesting observation from Fig. 4.4 is that the phase shift between ΔT_s and $\Delta \Omega_m$ is positive for perturbations with a frequency lower than the eigenfrequency. This should not surprise the reader, since the transfer function $\Delta \Omega_m/\Delta T_s$ is not dimensionless.

The results presented in Figures 4.1-4.4 can also be illustrated in another way. In the following simulated example the shaft torque varies sinusoidally between rated and zero for the 15 kW machine with some different frequencies. The machine will now respond as shown in Fig. 4.5.

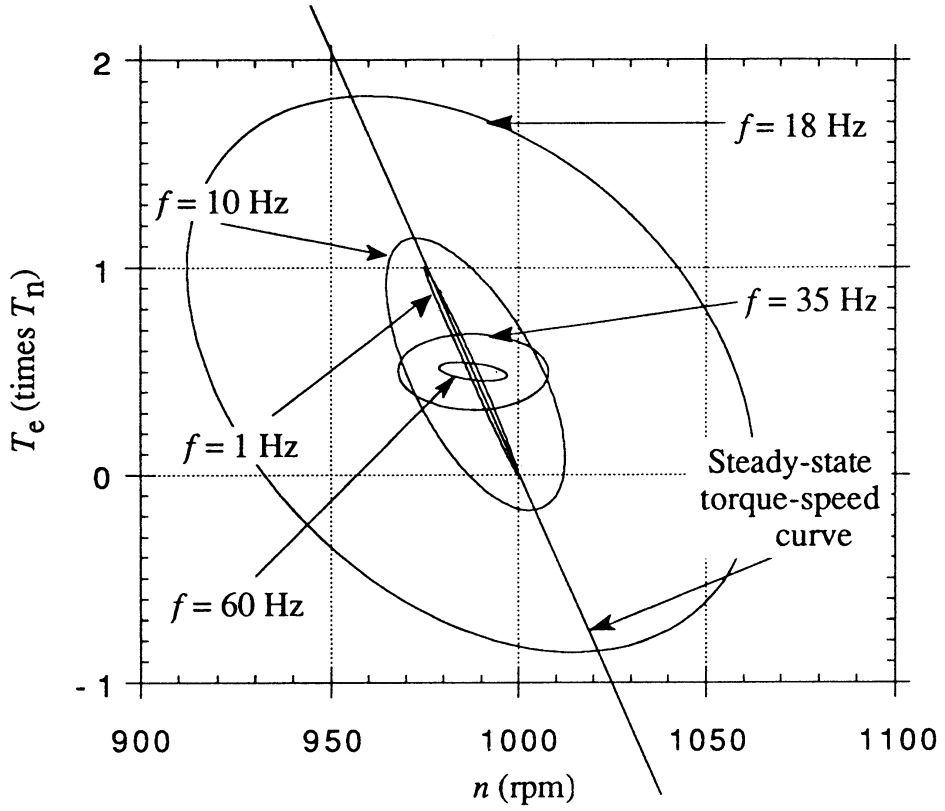

Figure 4.5. Induction machine response due to shaft torque perturbations of some different frequencies.

For very low disturbance frequencies the electrodynamical torque and the rotor speed follow the stationary torque-speed curve. As the frequency of the disturbances increases, the stationary torque-speed curve is no longer applicable.

4.2 Voltage pulsation

The supply voltage can either vary in amplitude or in frequency (phase). In the first case the supply voltage is amplitude-modulated

$$\underline{u}_S(t) = U(1 + \varepsilon \sin(2\pi f t))e^{j\omega_S t} \tag{4.1}$$

and in the second case frequency-modulated

$$\underline{u}_S(t) = Ue^{j\omega_{S0}(1 + \varepsilon \sin(2\pi f t))t} \tag{4.2}$$

where ε is the relative amplitude of disturbance and ω_{S0} is the steady-state supply angular frequency. No measurements are performed with voltage pulsations, only calculations. The resistance values at a cold machine are used and no compensation is performed for the skin effect in the rotor conductors. The selected operating-point is $T_n/4$ as a generator. The magnitude of the disturbance is small, $\varepsilon = 0.01$ ($\Delta U = 8$ V, $\Delta\omega_S = 0.5$ Hz).

4.2.1 Pulsations in the amplitude of the supply voltage

In Table 4.4 the models used to determine the response to pulsations in the amplitude of the supply voltage are presented.

Table 4.4. Models used to determine the response to perturbations in the amplitude of the supply voltage.

Model	Abbreviation	Equation(s)
Detailed model	Det-model	(2.18)
Small-perturbation model	SP-model	(2.29) and (2.30)
Non-linear damper model	ND-model	(2.23) inserted into (2.37)

Figures 4.6 and 4.7 present the gains and phase shifts of the transfer functions $\Delta T_e/\Delta U$ and $\Delta\Omega_m/\Delta U$ determined by means of the different models. It was not possible to derive NSR-models with the amplitude of the supply voltage as input as mentioned in Section 2.3.4.

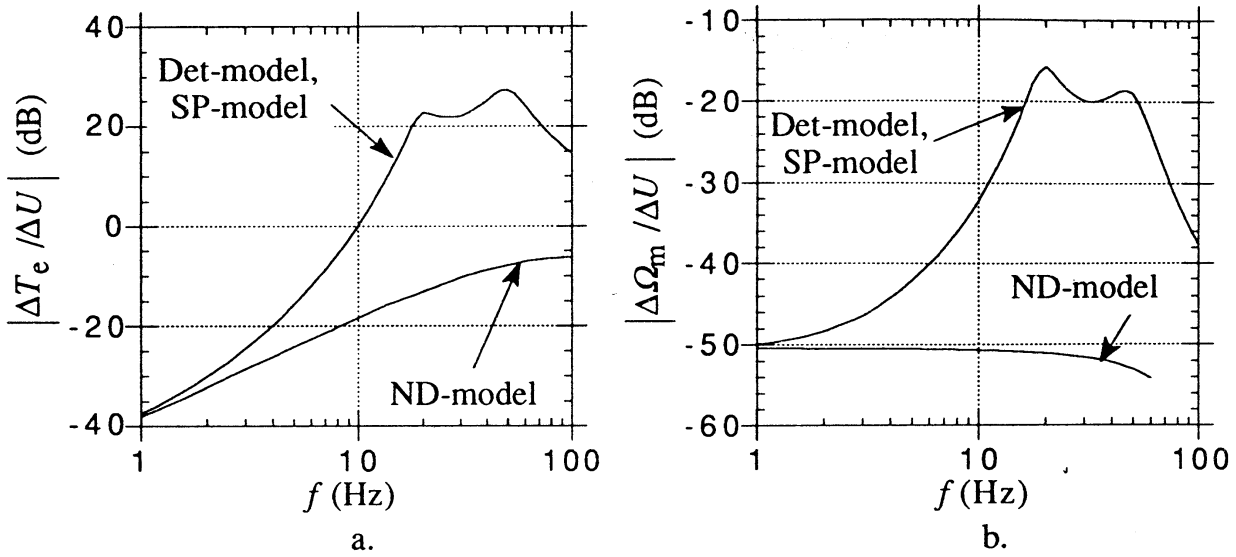

Figure 4.6. Calculated gains: a) $\Delta T_e/\Delta U$ b) $\Delta \Omega_m/\Delta U$

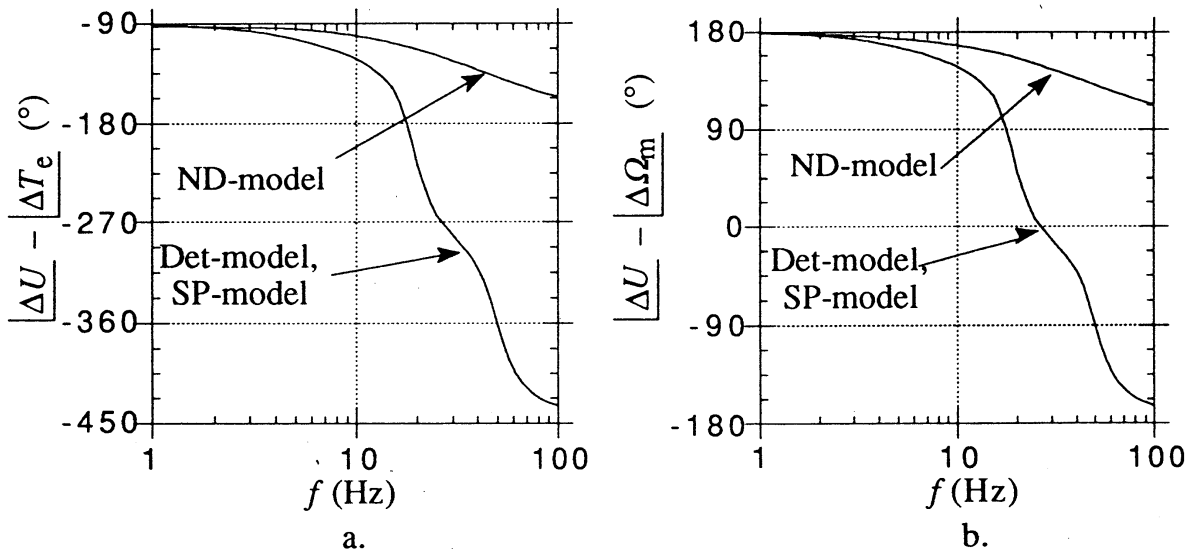

Figure 4.7. Calculated phase shifts: a) $\angle\Delta U - \angle\Delta T_e$ b) $\angle\Delta U - \angle\Delta \Omega_m$

The results from the small-perturbation model match well the results computed using the detailed model, since a small disturbance amplitude is used. Since the transfer function $\Delta T_e/\Delta U$ is an integration of the transfer function $\Delta \Omega_m/\Delta U$, the phase diagrams in Fig. 4.7 are identical with a difference of 90 °. Also in the case where the response to pulsations in the amplitude of the supply voltage is to be calculated, the use of a first-order model is limited to very low-frequency disturbances. The error in the prediction of the gains and phase shifts between the detailed model and the non-linear damper model is presented in Table 4.5.

Table 4.5. The discrepancy between the detailed model and the non-linear damper model in the predictions of the gain and phase shift of the voltage transfer functions.

f (Hz)	Gain discrepancy (dB)	Phase shift discrepancy (°)
0.5	–0.16 (2 %)	0
1	–0.58 (6.9 %)	–0.15
3	–4.1 (60%)	–3.1
5	–8.4 (163 %)	–7.8

From Table 4.5 it can be observed that the validity of the damper model is very limited in this case. Wasynczuk et al. [19] showed that it is possible to predict rather well the gain of $\Delta\Omega_m/\Delta U$ up to the dominating eigenfrequency with a third-order numerical model, at least in generator operation.

In Fig. 4.8 the response to sinusoidal perturbations of some different frequencies in the amplitude of the supply voltage of ΔU=8 V is presented. The calculation is performed on the 15 kW machine operating as a generator with a shaft torque of $T_n/4$.

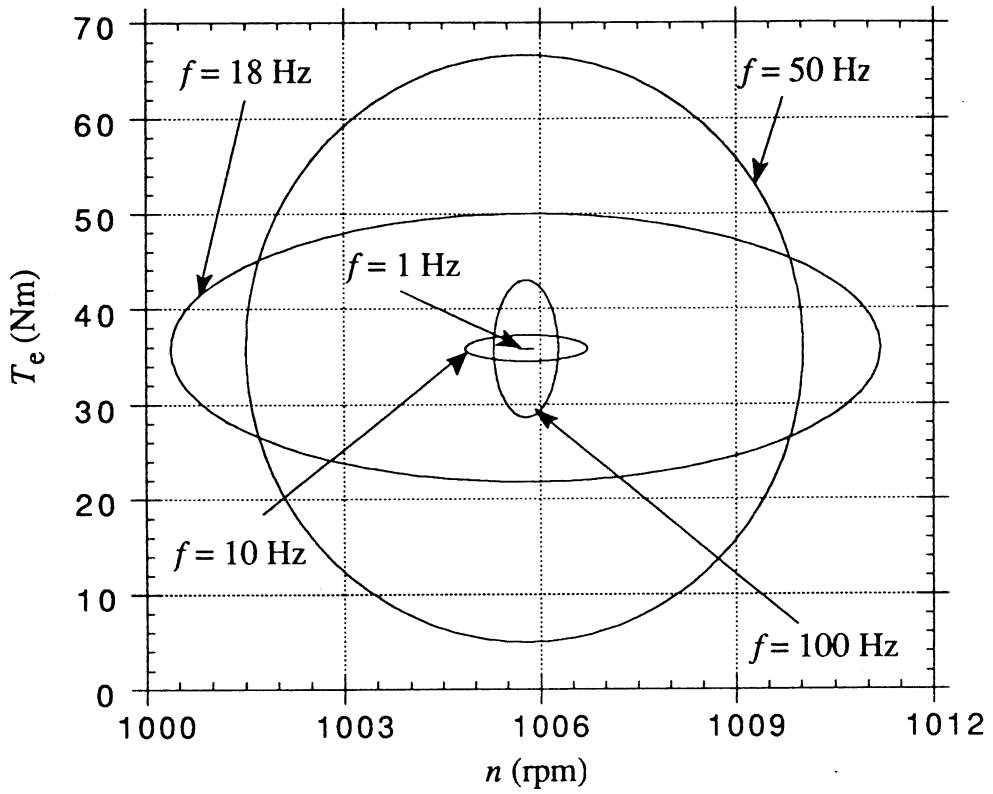

Figure 4.8. Induction machine response to a pulsating supply voltage amplitude.

For low-frequency perturbations, the slip (speed) of the machine slowly varies as the voltage pulsates in order to keep the electrodynamical torque constant. As the frequency of the pulsations increases, both the speed and the torque pulsate strongly. When the frequency of the voltage perturbations increases further, above the upper eigenfrequency, the oscillations will fall off.

4.2.2 Pulsations in the supply frequency

The models used to determine the induction machine response to perturbations in the frequency of the supply voltage are presented in Table 4.6.

Table 4.6. Models used to determine the response to perturbations in the frequency of the supply voltage.

Model	Abbreviation	Equations
Detailed model	Det-model	(2.18)
Small-perturbation model	SP-model	(2.32) and (2.33)
Neglecting Stator Resistance model	NSR-model	(2.48) and (2.49)
Non-linear damper model	ND-model	(2.23) inserted into (2.37)

Figures 4.9 and 4.10 show the ratios and phase shifts for the transfer functions $\Delta T_e/\Delta\omega_s$ and $\Delta\Omega_m/\Delta\omega_s$ calculated using different models.

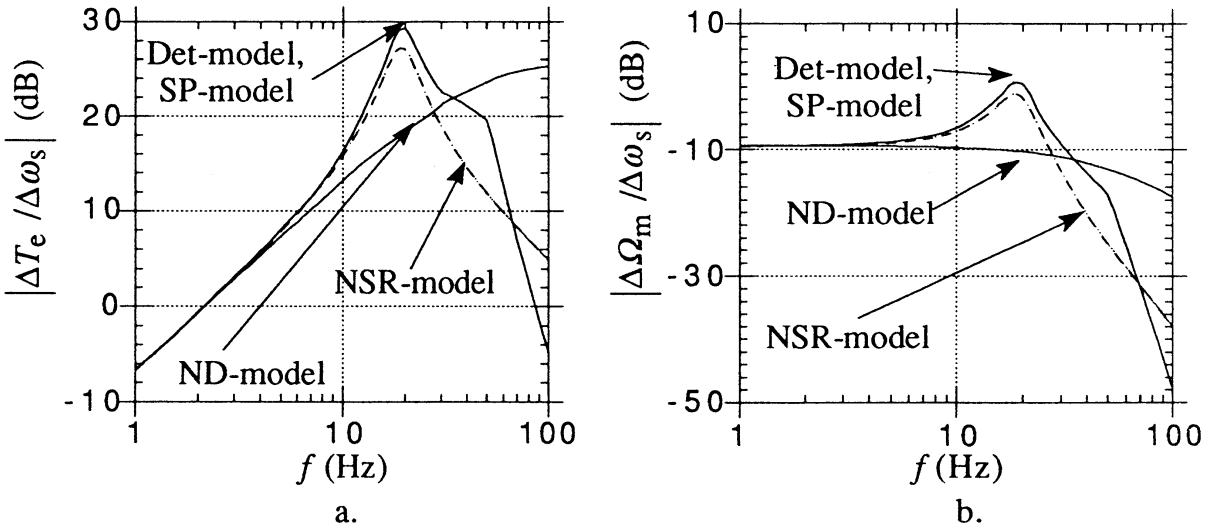

Figure 4.9. Calculated gains: a) $\Delta T_e/\Delta\omega_s$ b) $\Delta\Omega_m/\Delta\omega_s$

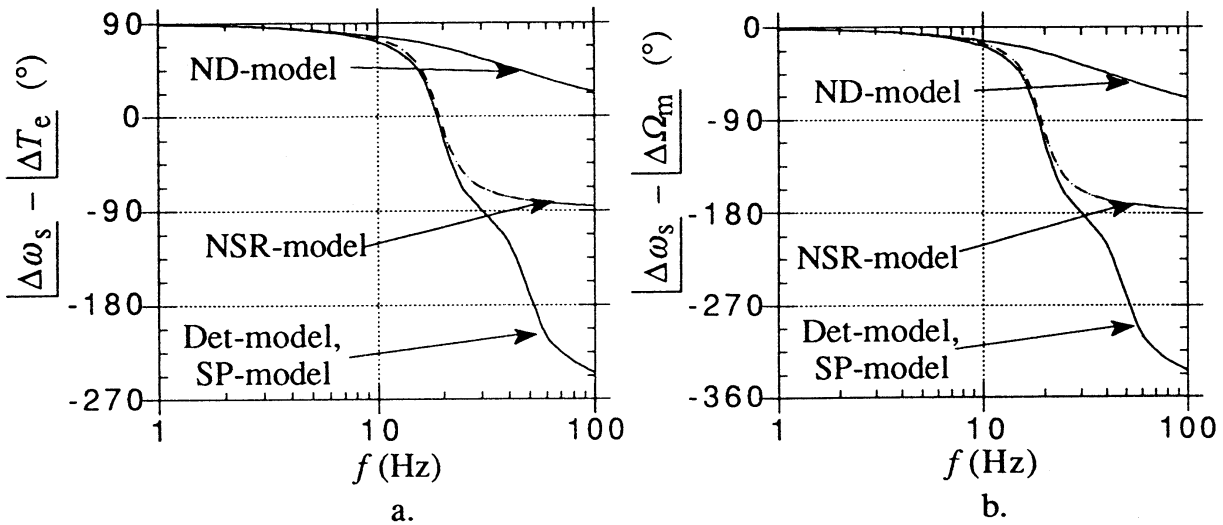

Figure 4.10. Calculated phase shifts: a) $\angle\Delta\omega_s - \angle\Delta T_e$ *b)* $\angle\Delta\omega_s - \angle\Delta\Omega_m$

The results are similar to the ones obtained in the previous case, where the response due to disturbances in the amplitude of the supply voltage was calculated. Also in this case a small disturbance amplitude has been used so the values predicted by the transient model and the small-perturbation model agree well. The prediction of the ratios and phase shifts obtained by means of the NSR-model resembles the result predicted using the detailed model up to the lower eigenfrequency. The most important difference is that the damping is over-estimated. The non-linear damper model is in this case capable of calculating the response of the machine for frequencies higher than in the case, where the amplitude of the voltage pulsated sinusoidally. Still, the error in the gain of ΔT_e, $\Delta\Omega_m/\Delta\omega_s$ is somewhat higher than in the case where the input is the disturbance in the shaft torque. However, the prediction of the phase shift is very good. The discrepancy between the results obtained by means of the damper model and the detailed model is presented in Table 4.7.

Table 4.7. The discrepancy between the detailed model and the non-linear damper model in the predictions of the gain and phase shift of the frequency transfer functions.

f (Hz)	Gain discrepancy (dB)	Phase discrepancy (°)
1	–0.03 (0.3%)	0
3	–0.27 (3.1 %)	0
5	–0.75 (9 %)	–0.1
10	–3.12 (43 %)	–5.5

In Fig. 4.11 the response to perturbations of some different frequencies in the frequency of the supply voltage of $\Delta\omega_s = 0.5$ Hz is presented. The calculation is performed on the 15 kW machine operating as a generator with a shaft torque of $T_n/4$.

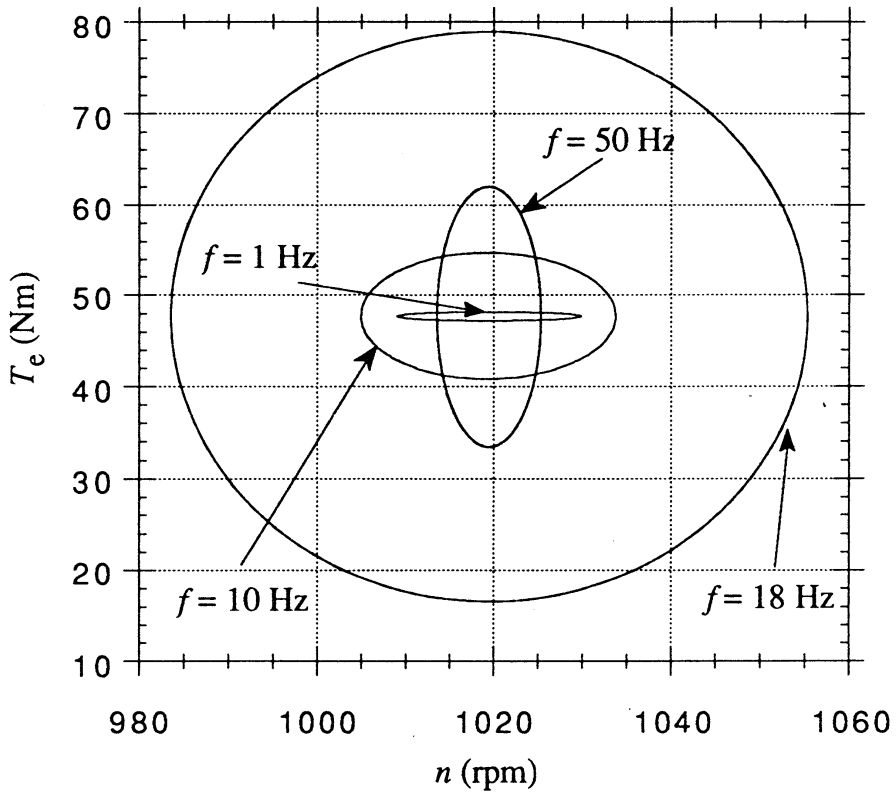

Figure 4.11. The response to a sinusoidally varying frequency of the supply voltage.

The machine adjusts the speed without any larger electrodynamical torque pulsations for slow frequencies, but as the frequency of the disturbance increases towards the lower eigenfrequency, the machine oscillations grow. As the frequency increases more, the oscillations are attenuated.

5 INFLUENCE ON THE DYNAMICS

5.1 Different disturbance amplitudes

In a linear system the gain is always independent of the disturbance magnitude. However, in a non-linear system this is not the case. For instance, in the induction machine, a large disturbance in the shaft torque will eventually cause the machine to pass the stall-point.

5.1.1 Torque pulsation

The difference between the response to a large and a small shaft torque perturbation increases as the static shaft torque increases. (The slope of the steady-state torque-speed curve decreases.) In Fig. 5.1 a calculated example is presented, in which a large and a small shaft torque pulsation are applied on the 15 kW machine operating as motor with an average shaft torque of 1.5 times the rated.

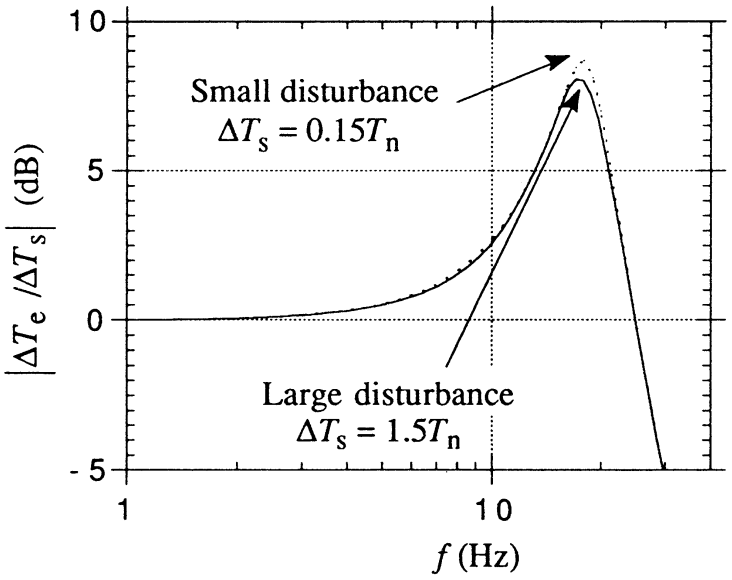

Figure 5.1. Calculated gain with different perturbation amplitudes for the 15 kW machine.

Although the rated operating-point has been passed, the difference in the gain of the transfer function $\Delta T_e/\Delta T_s$ is only detectable around the dominating eigenfrequency, where it is 0.6 dB = 7 %. In generator operation, where the slope of the steady-state torque-speed curve decreases less, the influence is even smaller.

5.1.2 Voltage pulsation

As a large pulsation in the supply voltage amplitude, 20% of the nominal grid voltage is selected. Figure 5.2 presents the response to a 7 Hz sinusoidal perturbation in the amplitude of the supply voltage of $\Delta U = 0.02U_n$ and $\Delta U = 0.2U_n$, respectively. The machine is operating as a motor with rated torque. The response to the small disturbance is amplified 10 times in order to obtain the same response magnitude.

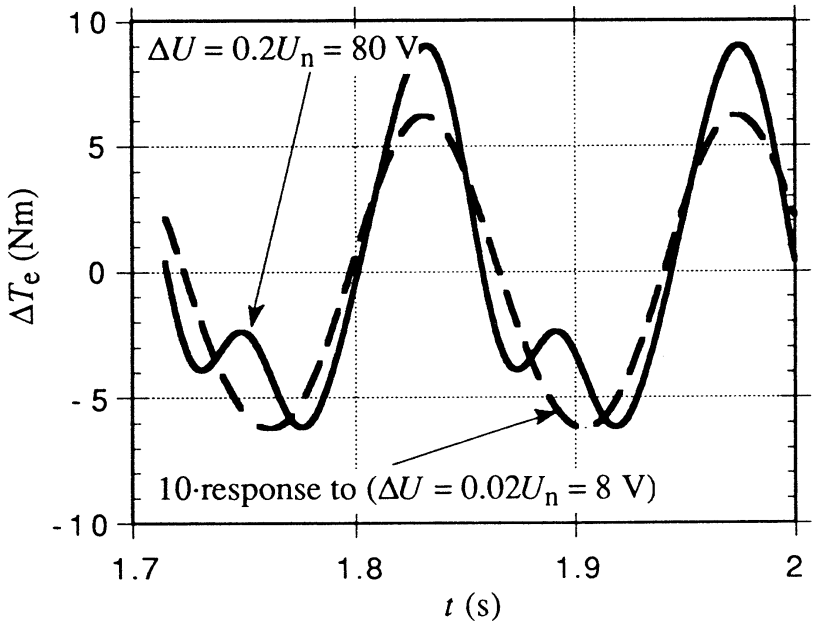

Figure 5.2. Torque response to a small (dashed curve) and a large (solid curve) perturbation in the supply voltage amplitude.

From Fig. 5.2 it stands clear that with a disturbance amplitude of 80 V, the linear analysis no longer predicts a good result.

If a small signal analysis is applied on (2.15) we get

$$T_e + \Delta T_e = p\,\mathrm{Im}(\underline{\Psi}_s^* \underline{i}_s + \underline{\Psi}_s^* \Delta \underline{i}_s + \Delta \underline{\Psi}_s^* \underline{i}_s + \Delta \underline{\Psi}_s^* \Delta \underline{i}_s) \tag{5.1}$$

and with the steady-state solution (2.14) subtracted

$$\Delta T_e = p\,\mathrm{Im}(\underline{\Psi}_s^* \Delta \underline{i}_s + \Delta \underline{\Psi}_s^* \underline{i}_s + \Delta \underline{\Psi}_s^* \Delta \underline{i}_s) \tag{5.2}$$

The last term in (5.2), small disturbance times small disturbance, is neglected in a small signal analysis which finally gives

$$\Delta T_e = p\,\mathrm{Im}(\underline{\Psi}_s^* \Delta \underline{i}_s + \Delta \underline{\Psi}_s^* \underline{i}_s) \tag{5.3}$$

Neglecting the last term in (5.2) works well in the case where the disturbance is 8 V, but in the second case this term is too large to be neglected.

The last term in (5.2) has a frequency of twice the disturbance frequency, 14 Hz. This second harmonic is clearly visible in Fig. 5.2.

5.2 Influence of machine parameters

The effect of the machine parameters on the dynamics of the machine, except for the stator resistance, can approximately be determined by examining (2.39) and (2.40). These equations indicate the damping at and the location of the dominating eigenfrequency for an induction machine. For a more detailed determination, small-signal analysis can be used if the disturbances are not too large. Figures 5.3 and 5.4 present the results from a small-signal calculation performed on the 15 kW machine operating as a generator with a shaft torque of 40 Nm.

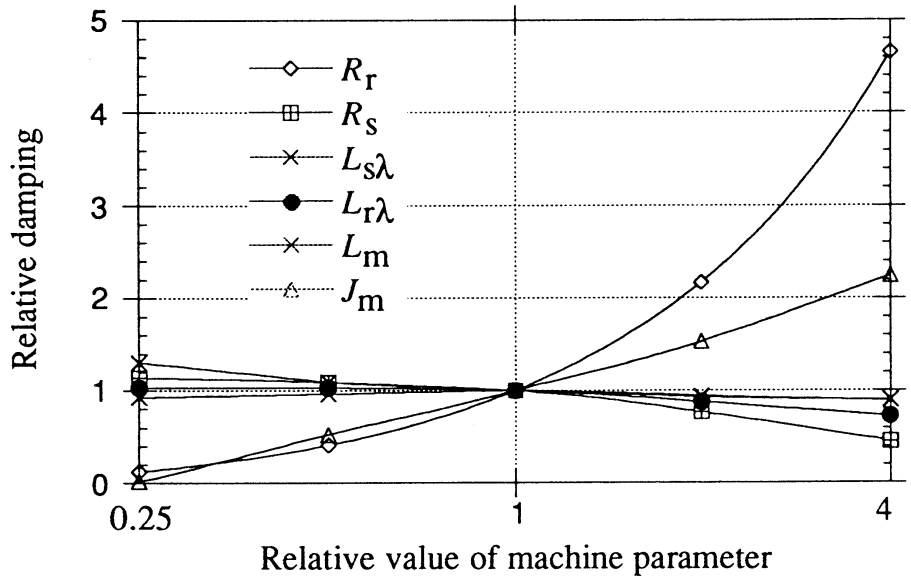

Figure 5.3. Damping with varied values of the machine parameters.

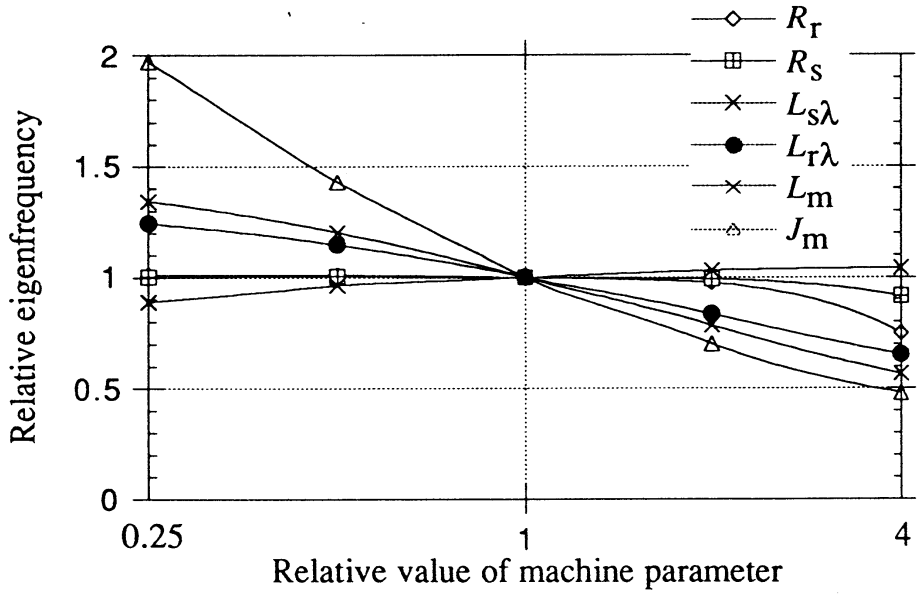

Figure 5.4. Eigenfrequency with varied values of the machine parameters.

The results approximately coincide with the results obtained by examining the NSR-models (2.39) and (2.40), but not exactly. For instance, a rotor resistance 4 times larger would according to (2.39) give a 4 times higher damping, but it gives a damping which is 4.6 times higher. Except for the rotor resistance, which effects the damping very strongly, the inertia also influences the damping. The influence of the other machine parameters can be neglected except for the stator resistance which usually causes a reduced damping for increasing values. The eigenfrequency is mainly effected by the inertia and the leakage inductances. As can be seen from Fig. 5.3, the damping is very low for a small inertia. With a machine inertia of 0.15 times the existing one, the damping ratio of the 15 kW machine will be negative leading to self-excited oscillations. That the inertia would be this small is not likely to happen, but the 15 kW machine can also oscillate for other combinations of machine parameters. For instance, if the machine is loaded with an extra inertia of 1.5 times the existing one and the stator resistance is 20 times the nominal one, the machine will respond to a small impulse disturbance according to Fig. 5.5.

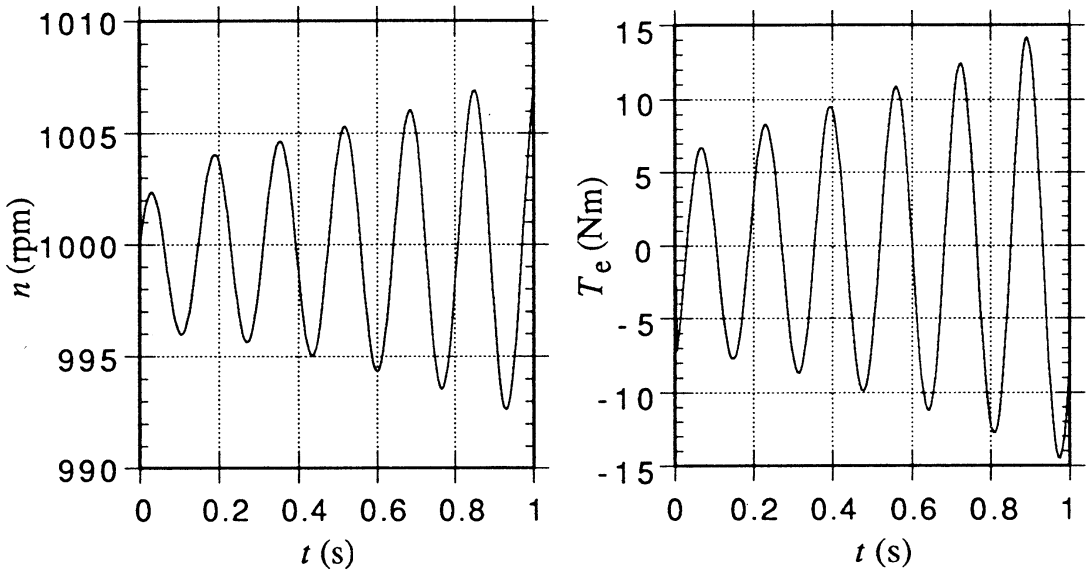

Figure 5.5. Self-excited oscillations of the 15 kW machine.

Instead of using different machines to verify the calculations with measurements, the parameters and operating variables of the 15 kW machine used are modified. For instance, the warming up of the machine is utilized to get a varied rotor resistance. External resistances and inductances are used in order to increase the stator resistance and stator leakage inductances and a lower supply voltage is used in order to reduce the flux level in the machine.

5.2.1 Leakage inductance

Increased stator leakage inductance mainly leads to lowered resonance frequency but also to reduced damping. Figure 5.6 shows the measured and calculated gain of $\Delta T_e/\Delta T_s$ for a stator leakage inductance of 2.2 mH and 6.4 mH. The machine is operating as a generator with a shaft torque of 43 Nm.

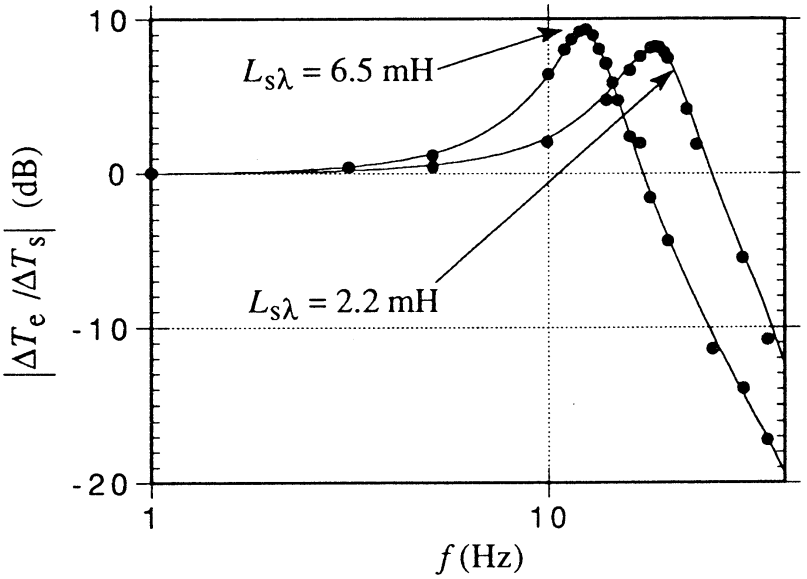

Figure 5.6. Gain of $\Delta T_e/\Delta T_s$ with different stator leakage inductances. The lines are calculated according to the detailed model and the dots are measured values.

5.2.2 Rotor resistance

The rotor resistance can not be directly measured. Instead a method is used in which the rotor resistance is determined by measuring the slip of the machine at some different times and using (2.36). The result is presented in Table 5.1.

Table 5.1. Measured slip and estimated rotor resistance at four different time points. The machine is operating as a motor with a shaft torque of 100 Nm.

t (min)	S	R_r
0	0.0145	0.19 Ω
10	0.0158	0.207 Ω
40	0.0173	0.227 Ω
180	0.0194	0.254 Ω

At the same time, the damping at the dominating eigenfrequency of the machine is determined from measurements obtained by using the PRBS-method. Figure 5.7 presents the gain of $\Delta T_e/\Delta T_s$ at some different time points.

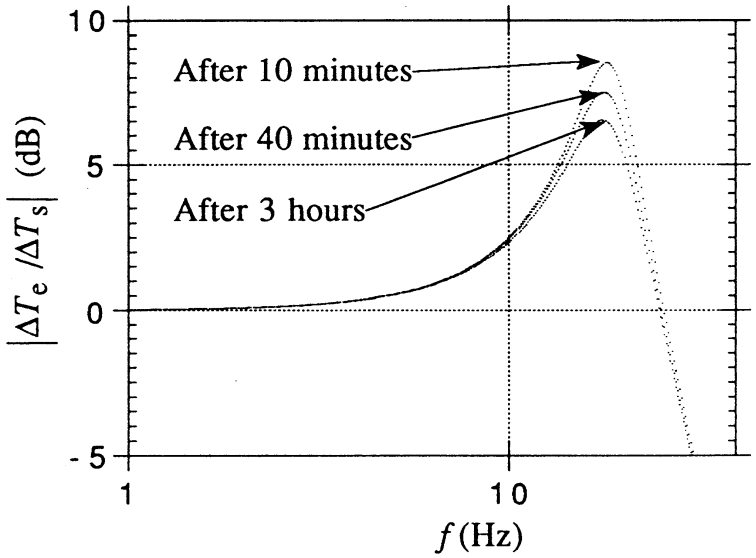

Figure 5.7. Measured gain of $\Delta T_e/\Delta T_s$ at different points of time.

The damping at the dominating eigenfrequency obtained by using the PRBS-method, is approximately proportional to the rotor resistance. The rotor resistance obtained by this method is the rotor resistance at the eigenfrequency, 19 Hz, which is 10 % higher than the low-frequency rotor resistance (See Fig. A.2). In Table 5.2 the dominant eigenvalues, and the estimated rotor resistances are presented.

Table 5.2. Estimated dominant eigenvalues and rotor resistances.

t (min)	dominant eigenvalues	estimated R_r (skin effect incl.)	estimated low-frequency R_r
2-3	$-22.8 \pm j117$	0.221 Ω	0.201 Ω
10	$-23.0 \pm j166$	0.230 Ω	0.209 Ω
40	$-26.5 \pm j115$	0.251 Ω	0.228 Ω
180	$-28.5 \pm j115$	0.277 Ω	0.252 Ω

The results predicted by means of the two methods coincide well except for the dc-value of the rotor resistance determined by using the PRBS-method directly after start which is too high.

5.2.3 The effect of stator resistance

In (2.39) and (2.40) the stator resistance is not included. At a supply frequency of 50 Hz, this is not of great importance for larger machines with a relatively small stator resistance. For smaller machines, though, the reduction of the damping due to the stator resistance cannot be neglected. For the investigated 15 kW machine the damping is reduced by 20 % due to the stator resistance. In some cases the damping can even be negative leading to self-excited oscillations as shown in Fig 5.5. If there is a series resistance, this must be included in the stator resistance when determining the stability of the machine. The results from measurements and calculations made on the 15 kW machine with $R_s = 0.25\ \Omega$ and $R_s = 0.80\ \Omega$ are presented in Fig. 5.8. The machine is operating as a generator with a shaft torque of 43 Nm.

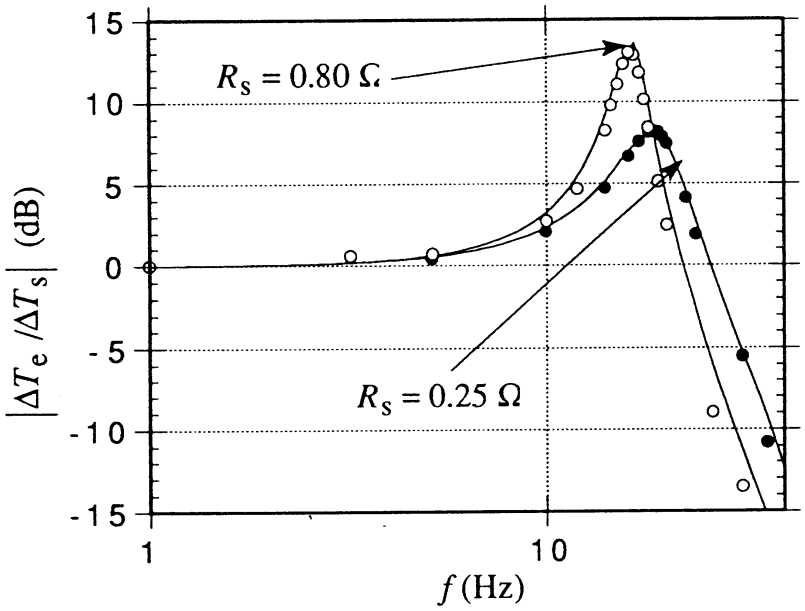

Figure 5.8. Gain of the transfer function $\Delta T_e/\Delta T_s$ with different stator resistances. The lines are calculations performed according to the detailed model and the dots and circles are measured values.

When the machine is operated with a converter, the resistance in the power switches, such as transistors or GTOs, must be added to the stator resistance, leading to reduced damping. Another important feature of power switches is that they have a voltage drop which has the same effects as an additional stator resistance. This might be of importance, especially at low currents.

Increased stator resistance does not automatically lead to reduced damping. For low supply frequencies the condition is usually the opposite. A growing stator resistance will always finally lead to increased damping. Normally, the induction machine has a certain stator resistance value for which the damping reaches a minimum or even becomes negative. As the stator resistance increases above this value, the damping is improved. For the 15 kW machine operating at 50 Hz the damping reaches a minimum for a stator resistance of 3.5 Ω with a damping ratio ξ = 0.0082. With this damping the amplification from shaft torque perturbation to perturbation in the electrodynamical torque at the dominating resonance frequency is 60 times larger than the low-frequency case. If the inertia of the machine had been 2.5 times the existing one, the damping would have been negative. The effect of this was demonstrated in Fig 5.5. At the upper eigen-frequency increasing stator resistance leads to improved damping.

The reason for the destabilizing effect of the stator resistance at the lower eigenfrequency can be found, if the stator flux is observed during a disturbance in the shaft torque. When the machine is disturbed by a pulsating shaft torque, both the reactive and active stator currents, oscillate, leading to an oscillation in the stator flux amplitude as well as in the stator flux phase due to the stator resistance. With a higher stator resistance the oscillation increases.

5.2.4 Flux level in the machine

The flux level in the machine is decreased by reducing the amplitude of the supply voltage without lowering the frequency. The purpose of reducing the flux level in the induction machine is that the efficiency can be improved when the static shaft torque is small. Figure 5.9 presents measurements and calculations on two different voltage levels, 230 V and 400 V. At 230 V the magnetizing inductance, L_m, is measured to be 44 mH. The 15 kW machine is operating as a generator with a driving shaft torque of 14 and 43 Nm, respectively, in order to obtain the same steady-state rotor speed.

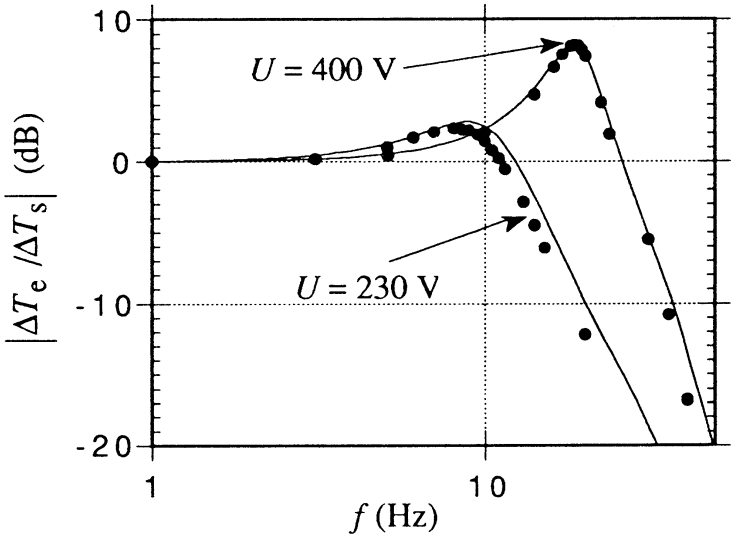

Figure 5.9. Gain of the transfer function $\Delta T_e/\Delta T_s$. Dots are measured values and lines are values calculated according to the detailed model.

The calculations of the 230 V case predict a somewhat lower damping and higher eigenfrequency than the measurements. The reason for this is unknown and has not been further investigated.

5.3 Variable frequency

When an induction machine is driven in variable-speed operation, the voltage is usually reduced in proportion to the frequency in order to keep the flux in the machine constant. If the proportion between the supply voltage and supply frequency is kept constant, the NSR-model (2.39) does not indicate that the dynamic behaviour should change as the supply frequency is varied. However, as seen in Fig. 5.10, which presents a calculated example made on the 15 kW machine operating as a generator with a driving shaft torque of 40 Nm, the damping and the resonance peak vary strongly.

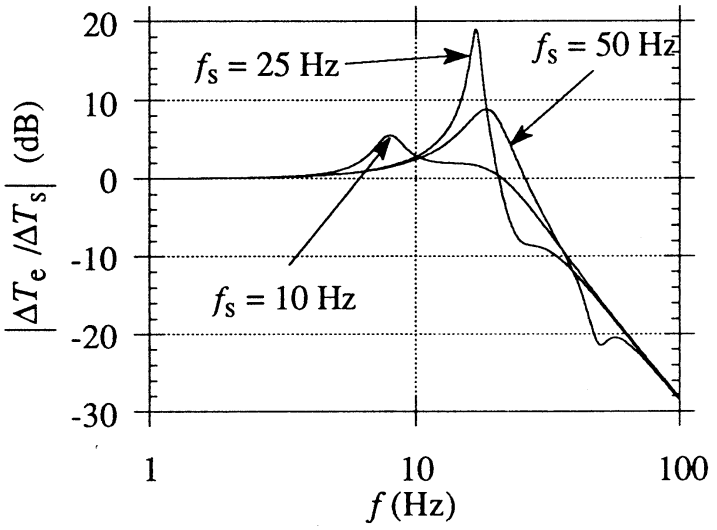

Figure 5.10. Gain of the transfer function $\Delta T_e/\Delta T_s$ for some different supply frequencies.

Again, it is the influence of the stator resistance which leads to different dynamic behaviour as the supply frequency varies. When the supply frequency is lowered, the stator resistance will be relatively larger compared to the reactances in the machine. Fig. 5.10 also shows that the NSR-model must be used with caution. Not even the second-order numerical model (2.25) works well at low supply frequencies. This is due to the fact that both eigenfrequencies play an important role on the induction machine dynamics at low supply frequencies.

5.4 The effect of different operating-points

5.4.1 Torque pulsation

Within the normal operating region of the machine, the dynamics is slightly influenced by the operating-point [12,18] as can be seen in the calculated example presented in Fig. 5.11.

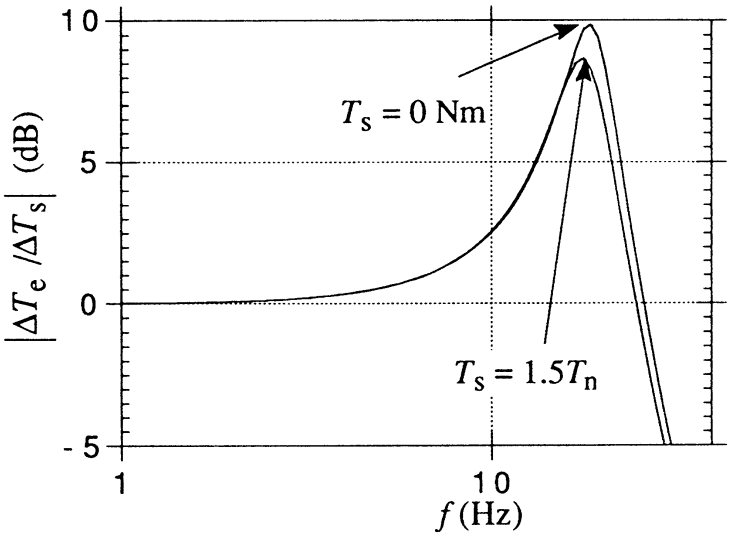

Figure 5.11. Gain of the transfer function $\Delta T_e/\Delta T_s$. The machine is operating as a motor with $T_S=1.5T_n$ and at no-load. Temperature variations are not taken into account.

In the normal operating region it is more important that the damping is improved with increasing temperature in the machine. As the temperature raises, the stator resistance increases which leads to reduced damping and the rotor resistance also grows leading to improved damping. The total effect is that the damping is increased as the temperature raises.

In Fig. 5.12 the calculated ratios of $\Delta T_e/\Delta T_s$ are presented for some different operating-points. The machine is operating as a motor, but the results are very much the same in generator operation.

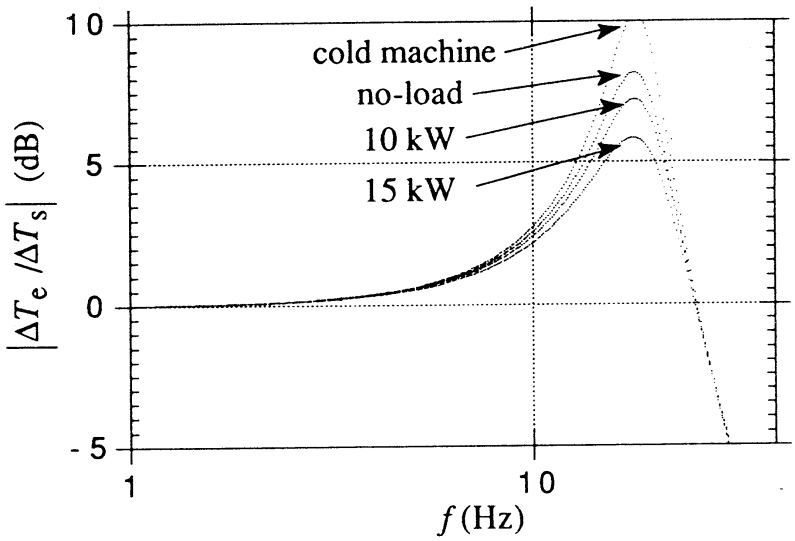

Figure 5.12. Gain of the transfer function $\Delta T_e/\Delta T_s$ at some different operating-points with temperature variations taken into account.

5.4.2 Voltage pulsation

Without taking temperature changes into consideration, the effect of the operating-point on the dynamics will be of little importance, if the shaft torque disturbance is the input. However, the influence of the operating-point is of large importance for the response to a disturbance in the amplitude of the supply voltage, even when temperature changes are not considered. In Fig. 5.13 the gain of the transfer functions $\Delta\Omega_m/\Delta U$ is compared in motor and generator operation.

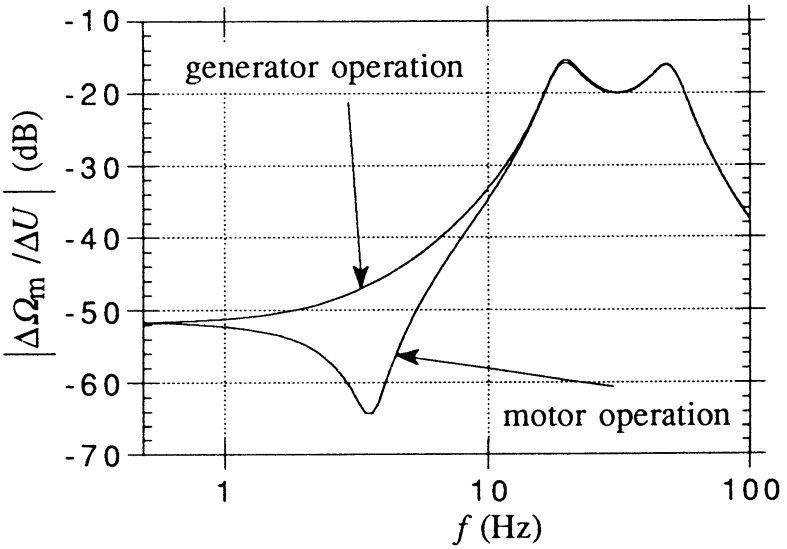

Figure 5.13. Gain of the transfer function $\Delta\Omega_m/\Delta U$ in generator and motor operation.

If small-signal analysis is used, the difference in the location of the zeros gives the explanation. In motor operation the linearized transfer function with the amplitude of the supply voltage as input, has a complex double zero. This does not exist in generator operation, where the transfer functions instead have one of the zeros in the right half of the s-plane (one of the zeros has a positive real part).

The location of the zeros for both motor and generator operation is presented in Fig. 5.14.

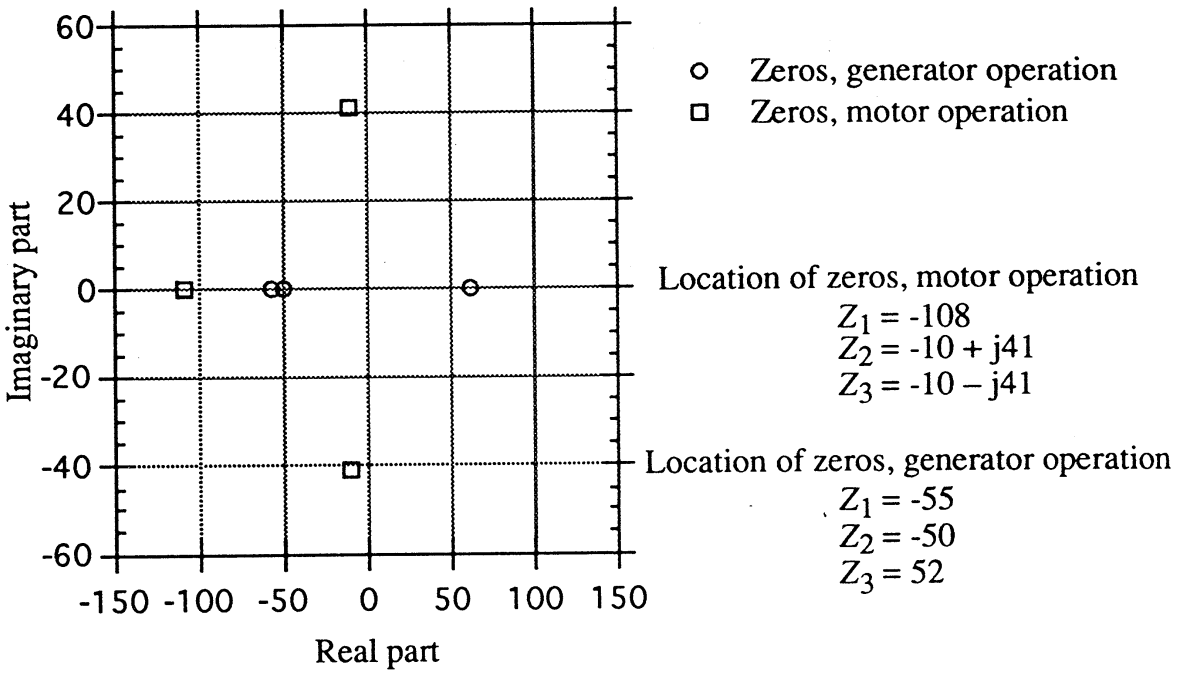

Figure 5.14. Zeros for the transfer function $\Delta\Omega_m/\Delta U$ in motor and generator operation.

The positive real part of one of the zeros indicates that the induction machine in generator operation will be a mixed phase system, if the input is a disturbance in the supply voltage amplitude. This can give special problems when controlling the machine in generator operation. The immediate response to a supply voltage increase is an increase of the rotor speed in generator as well as in motor operation. This is, however, the opposite direction towards the final value in generator operation, which is a decrease of the rotor speed. The physical explanation of this is that the immediate reaction on a raised voltage is that the current directed in the same axis as the voltage, i_{qs}, increases. This leads directly to a reduction of the rotor current in the quadrate axis, i_{qr}. Meanwhile, the rotor flux has not had time to change which means that the electrodynamical torque decreases, leading to a rotor speed acceleration in motor as well as in generator operation.

5.5 The influence of skin effect

The rotor conductors of a cage-bar induction machine are designed to give a higher resistance when the rotor current has a higher frequency in order to obtain a higher starting torque. This is done by utilizing the skin effect.

A torque disturbance on the shaft leads to a disturbance in the rotor current of the same frequency. Figure 5.15 shows a calculated case where the 15 kW machine is operating with rated shaft torque as a generator. The slip is 2% which gives a rotor current frequency of 1 Hz. This is represented by the dashed curve. In the second case, a sinusoidal shaft torque disturbance with a frequency of 18 Hz is applied, resulting in a rotor current with a ripple of 18 Hz. The rotor resistance is larger for this additional current. The solid line represents the rotor current in the second case.

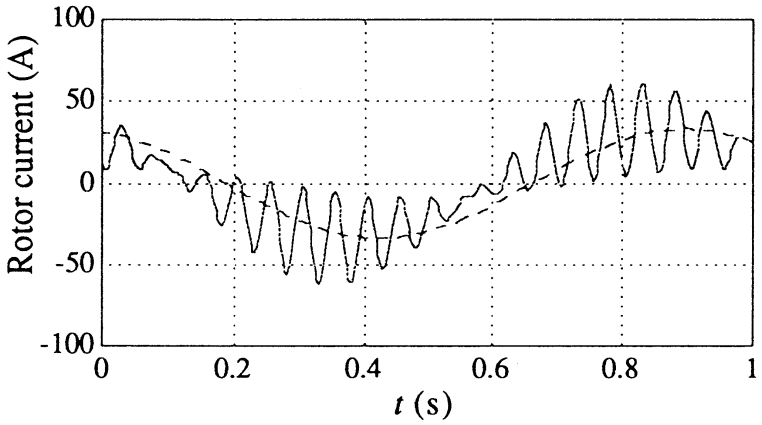

Figure 5.15. Calculated rotor currents. Dashed curve without a shaft torque pulsation and solid curve with a 18 Hz shaft torque perturbation.

Apart from the fact that the starting torque is raised by utilizing the skin effect, the damping is also increased as seen in Fig. 5.16.

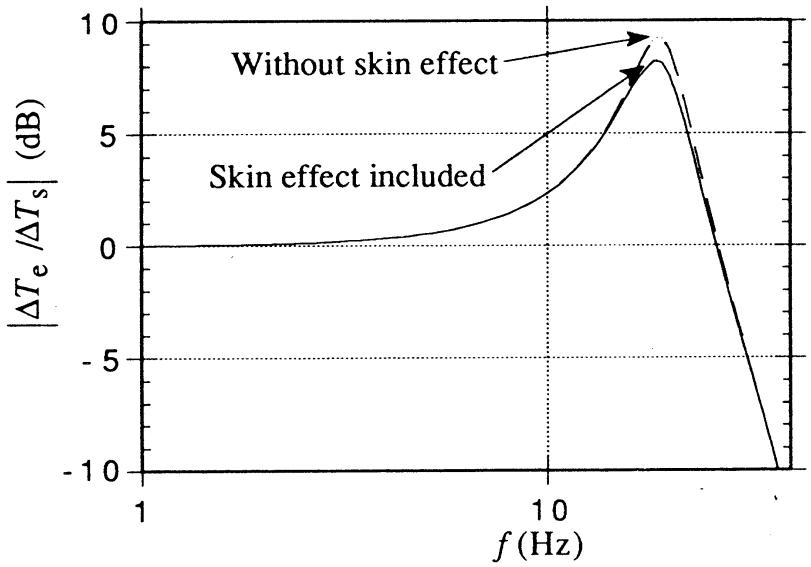

Figure 5.16. Calculated gain for the transfer function $\Delta T_e/\Delta T_s$ with and without skin effect taken into account.

At 18 Hz, which is the dominating resonance frequency of this machine, the rotor resistance is increased by 10 %, and consequently the damping is improved by 10 %. With a deep-bar rotor the increase of the rotor resistance will be larger. Meyer [17] found an increase of the damping of 20 % for a 3.1 MW machine with such conductors.

6 AN EXAMPLE WITH A NON-STIFF MACHINE SHAFT

The purpose of deriving linear and reduced order models of the induction machine is to simplify the analysis of the dynamics. With the NSR-model it is possible to analyse a larger system analytically, for instance the drive train of a wind turbine. Electric power pulsations from two-bladed wind turbines have been observed with a frequency twice the rotational frequency of the wind turbine. One reported example is the 2.4 MW wind turbine situated at Näsudden on the Island of Gotland in the Baltic Sea [1]. It has been suggested that these pulsations are caused by different wind speeds at different heights or due to the passing of the blades [2, 3]. The purpose of this section is not to analyse this specific problem but only to use it as a simple example. (The drive train of this wind turbine has been replaced during 1993.) The shaft of the large wind turbine on the island of Gotland had a torsional stiffness of $\alpha = 7.2 \cdot 10^8$ Nm/rad, including the gear-box. The turbine inertia, J_t, was $8.7 \cdot 10^6$ kgm^2 and the machine inertia, J_m, was 360 000 kgm^2 referred to the low speed side, see Fig. 6.1.

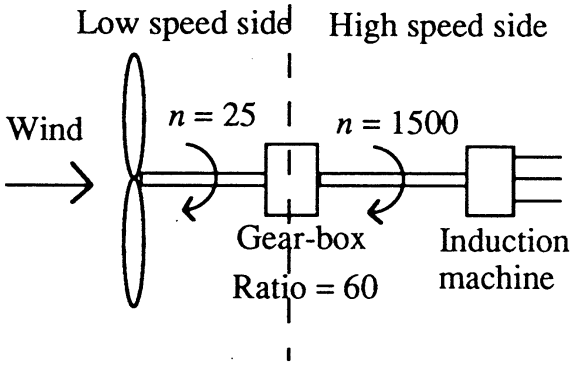

Figure 6.1. The drive train of the 2.4 MW wind turbine.

If the two masses are connected with a shaft having the torsional stiffness α and no damping, the undamped eigenfrequency of the two-mass system will be

$$f_0 = \frac{1}{2\pi}\sqrt{\frac{\alpha(J_m + J_t)}{J_m J_t}} \tag{6.1}$$

This gives an approximate value of the shaft eigenfrequency of 7 Hz.

A more accurate calculation of the shaft eigenfrequency can be made by determining the small-perturbation transfer functions of the system or a direct non-linear simulation.

If the NSR-model is used as the induction machine together with the soft shaft and wind turbine rotor, the following simplified model of the whole system will be obtained, see Fig 6.2.

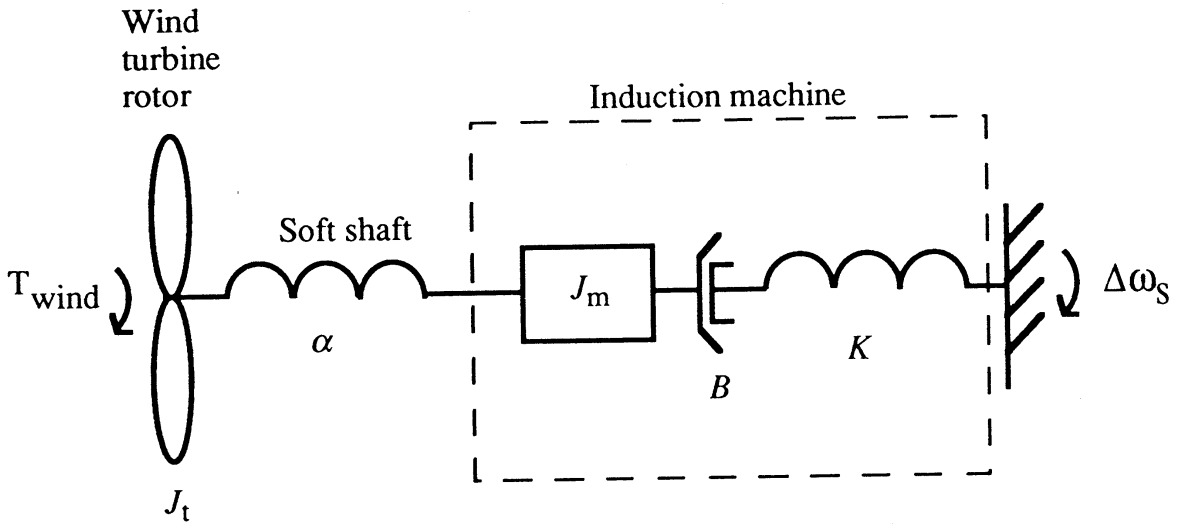

Figure 6.2. NSR-model connected with a wind turbine rotor via a soft shaft.

The linearized analytical transfer function $\Delta T_e/\Delta T_{wind}$ can now be derived.

$$\frac{\Delta T_e}{\Delta T_{wind}} = \frac{K}{s^4\frac{J_t J_m}{\alpha} + s^3\frac{J_m J_t K}{B\alpha} + s^2(J_m + J_t(1+\frac{K}{\alpha})) + s\frac{KJ_t + KJ_m}{B} + K} \qquad (6.2)$$

It is also possible to analyse the response to frequency disturbances. For instance, the simplified transfer function $\Delta T_e/\Delta\omega_s$ is

$$\frac{\Delta T_e}{\Delta\omega_s} = \frac{s^3\frac{J_t J_m}{\alpha} + s(J_m + J_t)}{s^4\frac{J_t J_m}{\alpha} + s^3\frac{J_m J_t K}{B\alpha} + s^2(J_m + J_t(1+\frac{K}{\alpha})) + s\frac{KJ_t + KJ_m}{B} + K} \qquad (6.3)$$

The gain of the transfer function $\Delta T_e/\Delta T_{wind}$ predicted with the NSR-based model and a model based on the detailed model are presented in Fig. 6.3 for the 2.4 MW wind turbine with the torsional stiffness varied.

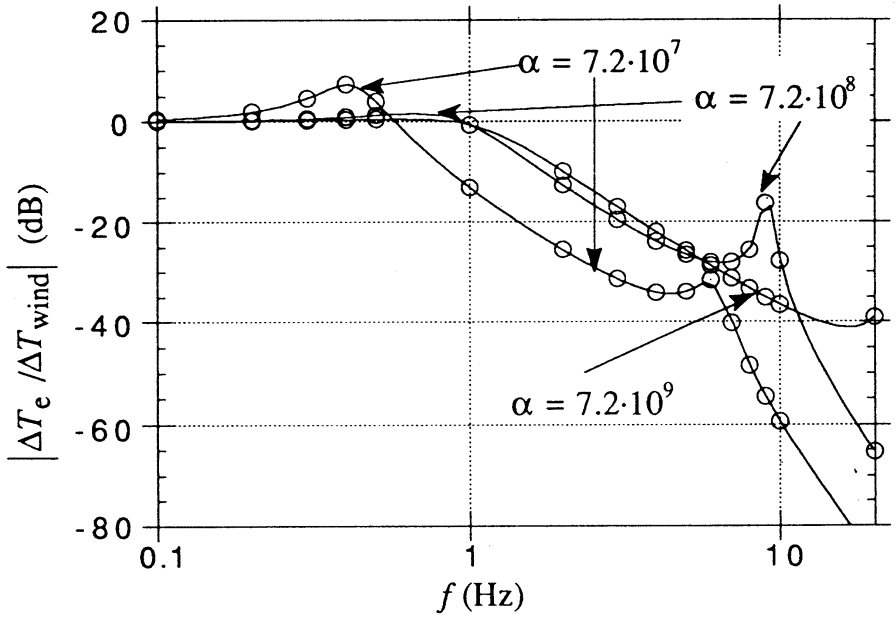

Figure 6.3. The gain of the transfer function $\Delta T_e/\Delta T_{wind}$ with varied shaft torsional stiffness. Solid curves are values determined by the NSR-based model and circle values determined with the detailed model.

As can be observed in Fig. 6.3, the NSR-based model predicts almost the same result as the detailed model. When the shaft is very soft, $\alpha = 7.2 \cdot 10^7$, disturbances around 0.4 Hz are amplified up to 7 dB, 2.2 times. The dominating eigenfrequency for this machine without load, 5.6 Hz (Table 2.3), can also be observed. For the case of $\alpha = 7.2 \cdot 10^8$ it can be noted that a disturbance in the wind torque with a frequency of 0.4-1 Hz is slightly amplified. The eigen-frequency between the machine and the wind turbine rotor inertia can be observed, 9 Hz (7 Hz computed using (6.1)).

7 CONCLUSION

In this thesis the low-frequency response of the induction machine has been investigated. The validity of results obtained by using linear analysis has been examined. For instance, the influence of varying machine parameters, different disturbance amplitudes, different operating-points, and the importance of the skin effect have been analysed. The results obtained have been used to give some guide-lines to when the induction machine can be represented by a simpler model.

The measured response to pulsations in the shaft torque can be very well predicted with the two-axis model, even if the non-sinusoidal distribution of the windings and saturation are not taken into account. It is important to take temperature variations into consideration, while corrections for skin effect seem to be of moderate importance for an ordinary industrial motor.

It was found that a first-order model can be used to determine the dynamic response to shaft torque or supply frequency disturbances up to a disturbance frequency of one or a few hertz, depending on the desired accuracy. The frequency region in which a first-order model can be used is even smaller when the response to disturbances in the amplitude of the supply voltage is to be calculated. The NSR-model (a second-order model derived by neglecting the stator resistance) can predict the response to shaft torque and supply frequency disturbances rather well providing that the stator resistance is low and that the supply frequency is not too low. If the stator resistance is too high, the damping will be over-estimated. The damping can be well predicted with a second-order numerical model also for smaller machines where the stator resistance usually is comparatively large. For low supply frequencies none of the second-order models work well, since both the eigenfrequencies then play an important part on the low-frequency dynamics of the machine.

The low-frequency dynamics of the machine is governed by the dominating eigenfrequency, provided that the supply frequency is not too low. In this investigation it was found that increasing stator resistance usually leads to reduced damping.

Finally an example was demonstrated where the NSR-model is used to derive analytical transfer functions for the whole drive train of a wind turbine.

8 REFERENCES

1 Svensson, G. (ed), Report from fullscale evaluation on the Swedish wind turbine prototype Näsudden. Swedish State Power Board. (Vattenfall), Stockholm, Sweden 1986 (In Swedish)

2 Hinrichsen, E.N., Nolan, P.J., Dynamics and stability of wind turbine generators. IEEE Transactions on Power Apparatus and Systems PAS-101(1982)8, p. 2640-2648

3 Chan, S.M., Cresap, R.L., Curtice, D.H., Wind turbine cluster model. IEEE Transactions on Power Apparatus and Systems PAS-103(1984)7, p. 1692-1698

4 Nacke, H., Schwingungsverhalten des Asynchronmotors. ETZ-A 83(1962)24, p. 793-797

5 Lorenzen, H.W., Angefachte Eigenschwingungen von Drehstrom-Asynchronmaschinen. Brown Boveri Mitteilungen 55(1968)10/11, p. 650-663

6 Novotny, D.W., Melkebeek, J.A.A., Dynamic response of voltage-driven induction machines. Electric Machines and Power Systems 10(1985), p. 149-176

7 Lorenzen, H.W., Die erzwungenen Schwingungen von Asynchronmotoren unter Berücksichtigung des Ständerwiderstandes. ETZ-A 88(1967)8, p. 195-202

8 Lorenzen, H.W., Das transiente Verhalten und die dynamische Stabilität von symmetrischen Drehstromasynchronmaschinen bei veränderlicher Primärfrequenz. Bull. SEV, 62(1971)4, p. 237-246

9 Nelson, R.H., Lipo, T.A., Krause, P.C., Stability analysis of a symmetrical induction machine. IEEE Transactions on Power Apparatus and Systems PAS-88(1969)11, p. 1710-1717

10 Palit, B.B., Eigenwertuntersuchungen an einer Drehstrom-Asynchronmaschine bei selbsterregten Drehschwingungen. Bull. SEV/VSE 69(1978)8, p. 371-376

11 Kron, A.W., Lorenzen, H.W., Die selbsterregten Pendelungen von Drehstrom-Asynchronmaschinen. ETZ-A 90(1969)9, p. 200-205

12 Freise, W., Jordan, H., Nacke, H., Experimentelle Ermittlung der erzwungenen Pendelungen von Drehstrom-Asynchronmaschinen. ETZ-A 85(1964)12, p. 370-372

13 Peterson, B., Oscillations in inverter fed induction motor drives. Licentiate thesis, Lund Institute of Technology 1991

14 Späth, H., Die Pendeleigenfrequenz am starren Netz betriebener Drehstromasynchronmaschinenantriebe und deren Messung. ATM 8(1974), p. 27-32

15 Leonhard, A., Die Asynchronmaschine bei periodischen und sprungartigen Belastungsänderungen. Elektrotechnik und Maschinenbau 83(1966)6, p. 357-359

16 Lorenzen, H.W., Der Einfluß der Stromverdrängung auf die erzwungenen Pendelungen von Asynchronmaschinen. ETZ-A, 88(1967)18, p. 445-451

17 Meyer, A., Einfluss der Stromverdrängung auf den stationären Betrieb und die erzwungenen Pendelungen von Asynchronmaschinen. Brown Boveri Mitteilungen, 63(1976)8, p. 500-507

18 Kovacs, P.K., Transient phenomena in electrical machines. Elsevier, Budapest 1984

19 Wasynczuk, O., Diao, Y.M., Krause, P.C., Theory and comparison of reduced order models of induction machines. IEEE Transactions on Power Apparatus and Systems PAS-104(1985)3, p. 598-606

20 Ljung, L., Glad, T., Kompendium i modellbygge och simulering. Linköping University, Sweden 1991 (In Swedish)

21 Lennartson, B., Otteblad, A., Formelsamling i reglerteknik. Chalmers University of Technology, Sweden 1983 (In Swedish)

22 Langheim, J., Modelling of rotorbars with skin effect for dynamic simulation of induction machines. IEEE Inductry Applications Society Annual Meeting, 1-5 October 1989, San Diego, p. 38-44

23 Bose, B.K., Power electronics and AC drives. Prentice-Hall, New Jersey 1986

24 Narraway, J.J., Eigenvalues of the state matrix for an induction machine. J. Franklin Inst (USA), Vol. 300(1975), p. 75-78

25 Policastro, M., Torriano, D., On the location of the eigenvalues of a generalized model of the asynchronous machine. Int. Journal of Modelling & Simulation 7(1987)2, p. 72-76

26 Lorenzen, H.W., Das dynamische Betriebsverhalten von Asynchronmaschinen bei kleinen Abweichungen vom stationären Zustand. Brown Boveri Mitteilungen 56(1969)11/12, p. 548-569

27 Proakis, J.G., Manolakis, D.G., Introduction to Digital Signal Processing. Macmillan Publishing Company, New York 1988

28 Ljung, L., System Identification - Theory for the User, Prentice-Hall Englewood Cliffs, N.J., 1987

APPENDIX A DETERMINATION OF THE ROTOR RESISTANCE OF THE 15 KW MACHINE

The rotor resistance is usually determined from the locked-rotor resistance

$$R_k \approx R_S + \left(\frac{L_m}{L_m + L_{r\lambda}}\right)^2 R_r + R_{cl} \tag{A.1}$$

where R_{cl} is an equivalent to the core losses. R_{cl} is usually not taken into account which means that the determined rotor resistance value will be somewhat too high. With a different method it is possible to obtain a more accurate rotor resistance value.

The locked rotor current I_r can be determined from the simplified equivalent circuit

$$I_r = \sqrt{\frac{U_0^2}{(R_0 + R_r)^2 + X_0^2}} \tag{A.2}$$

With (A.2) inserted into (2.23) the electrodynamical torque expression becomes

$$T_e = \frac{3pR_r}{\omega_s} I_r^2 \tag{A.3}$$

By rearranging (A.3) the rotor resistance can be expressed as

$$R_r = \frac{\omega_s T_s}{3pI_r^2} \tag{A.4}$$

since $T_s = T_e$. With the knowledge of the voltage, current, power factor, frequency and shaft torque the rotor resistance is determined by using an iteration procedure in which (2.18), (A.4) and (A.1) are involved.

The measurement set-up to determine the rotor resistance is presented in Fig. A.1.

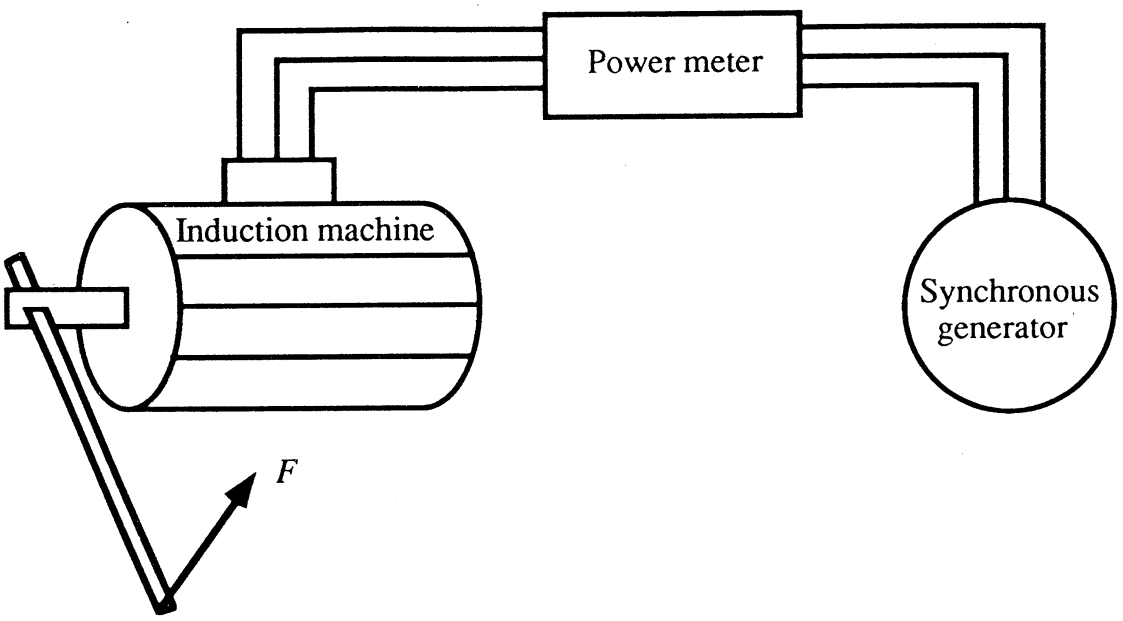

Figure A.1. The measurement set-up during the locked rotor test.

The locked rotor test is performed on different voltage levels and at different supply frequencies. Throughout the locked rotor test measurements, the machine temperature is kept constant. The variable frequency variable voltage source is produced by a synchronous generator in order to obtain a low harmonic content. The voltages, currents, frequency and power factor are measured with a power meter (Yogogawa 2533). The torque is calculated by measuring the force F with a dynamometer (MESK, 10 N) at the end of a lever. The locked-rotor torque is determined as the average torque over one cogging period. The current levels are kept below the rated current in order not to saturate the machine. The measured values of the rotor resistance are presented in Fig. A.2.

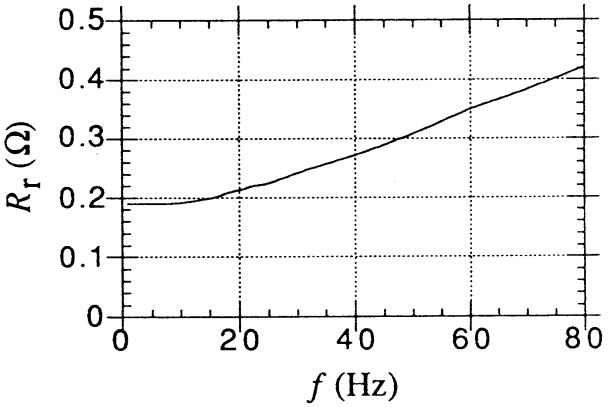

Figure A.2. Measured rotor resistance.